Micro-Raman Imaging of Heterogeneous Polymer Systems: General Applications and Limitations

LARS MARKWORT* and BERT KIP

DSM Research, PO Box 18, 6160 MD Geleen, The Netherlands

SYNOPSIS

This article assesses the use of micro-Raman imaging with respect to polymer science. This relatively novel technique allows, at high spatial resolution, the acquisition of chemical and morphological information over an area of a sample. Using Raman imaging by confocal laser line scanning, a wide range of problems in polymer analysis has been studied to outline the capabilities and limitations of the technique. Three ternary polymer blends consisting of polypropene/polyethene/ethene–propene copolymer, polybutyleneterephthalate/polycarbonate/very low density polyethene, and styrene-*co*-acrylonitrile/styrene-*co*-maleicanhydrate/poly-2,6-dimethylphenylene oxide were studied with regard to compositional and morphological heterogeneities. In a binary polymer blend consisting of two different acrylate monomers, the refractive index profile established after artificially induced diffusion of the main components was determined from the concentration gradients. The distribution of unreacted free melamine in a cured melamine–formaldehyde resin was analyzed. Furthermore, the general structure of a composite sample consisting of polyethene fibers in an epoxide matrix was studied. Raman imaging proved suitable for the characterization of heterogeneities in composition and morphology on a size scale equal to or larger than 1 μm. In this sense, the technique helps to close the gap between infrared microscopy, with its comparatively poor spatial resolution, on the one hand, and transmission electron microscopy, with its limited chemical information, on the other hand. For heterogeneities on a submicron scale, the value of the technique is limited to the determination of average information. When combined with curve fitting, Raman imaging permitted us to determine the composition of the polypropene/polyethene/ethene–propene copolymer blend with an accuracy of 5–10%. The main limitations to micro-Raman imaging of polymer systems based on the confocal laser line scanning technique have been identified as the destruction of the samples due to insufficient heat dissipation of the high-incident laser power, interferences due to fluorescence, and the stability of the instrumentation during long collection times required for good signal-to-noise ratio spectra of weak Raman scatterers.

INTRODUCTION

The development of polymer products with specific material properties often involves the compounding with additives such as fillers, stabilisers, other polymers, foaming agents, etc.[1,2] Frequently, inhomogeneities in composition and morphology arise in the compounded polymer system. It is generally believed that the overall material properties of a polymer blend material depend to a large extent on the microscopic inhomogeneities prevalent.[3-6] For a better understanding of the influence of the inhomogeneities on the material properties, it is desirable to obtain information of the sample at a high spatial resolution. Although visible light or electron microscopical techniques are used extensively for the structural characterization of polymer blends, they often fail to provide unambiguous identification of the individual phases in the sample. Furthermore, the extraction of quantitative data are seldom feasible.

* To whom correspondence should be addressed.

Journal of Applied Polymer Science, Vol. 61, 231–254 (1996)
 CCC 0021-8995/96/020231-24

To obtain directly the desired chemical and morphological information at high spatial resolution, infrared and Raman microscopy appear suitable techniques. Both Raman and infrared spectroscopy are prominent in the analysis of polymers, since they can yield a unique molecular fingerprint which contains information on the type and quantity of molecules prevalent, their structure (configuration and conformation), and the local environment they are in (i.e., amorphous or crystalline, oriented or unoriented[7-9]). Compared to the extensively used infrared spectroscopy, Raman spectroscopy has a number of decisive disadvantages (i.e., the relative weakness of the Raman effect and the susceptibility of the technique to fluorescence). Generally, one applies infrared spectroscopy to molecular fingerprinting problems. However, Raman spectroscopy has a number of characteristics which make its use interesting for the chemical analysis at high spatial resolution. Most commonly, visible or near infrared laser light is used to excite the Raman scatter, and it is possible to use an ordinary optical light microscope as the excitation beam condenser and at the same time collect very efficiently the backscattered Raman light[10-14] for a subsequent spectral analysis. The main advantage in this context is the possibility to focus the probing laser beam to spot sizes of the order of 1 μm. A spatial resolution considerably higher is thus achievable with Raman as compared to infrared microscopy. Generally, it can be said that provided the sample under investigation is not fluorescent or light sensitive, the Raman spectroscopic analysis is relatively straightforward. No particular sample preparation is necessary,[15] and sample alignment and focusing onto microscopic features in or on the sample are easy. Furthermore, the collection of the Raman scatter can be made confocal, improving lateral and depth spatial resolution significantly.[16-20] By discriminating the extraneous light contributed by out-of-focus objects, the image contrast is dramatically improved. With a confocal microscope, it is possible to obtain sharp images of focal planes on the surface of or immersed in thick objects.[17,21,22] Confocal Raman microscopy is now conveniently applied to point analysis and depth profiling of chemical and structural inhomogeneities, molecular orientation, and local stress.[23,24]

More recently, the efficient Raman analysis of whole areas of a sample has become a viable option by the development of Raman imaging. There are three principally different Raman imaging concepts based on conventional Raman spectroscopy. The differences are essentially based on the form of sample illumination used to excite the Raman scatter (i.e., point-by-point sampling, line sampling, and real-time imaging of light distribution in a wide-field (globally) illuminated sample area). The different imaging concepts have, to more or less extent, been the subject of previous articles.[23,25-27] The comparison of the different Raman imaging techniques with respect to polymer analysis revealed that the technical realization of Raman imaging by confocal laser line scanning is suited best for a general application in polymer science.[28] This technique was chosen here to demonstrate the value of Raman imaging for the study of heterogeneities in polymer systems. Three different ternary polymer blends were studied with respect to compositional and morphological heterogeneities. In a binary polymer blend consisting of two different acrylate monomers, the refractive index profile was established from the concentration gradients after thermally induced diffusion of the components. The distribution of unreacted free melamine in a cured melamine–formaldehyde resin was analyzed. Furthermore, the general structure of a composite sample consisting of polyethene fibers in an epoxide matrix was studied.

EXPERIMENTAL

Raman Instrumentation

A Dilor XY800 spectrometer was used with a double monochromator in subtractive mode for the rejection of stray light and Rayleigh scatter and a third monochromator for energy dispersion (1800 grooves/mm grating, f = 800 mm). The entrance slit was set to 150 μm corresponding to 3 cm^{-1} spectral resolution. A Spectra Physics Ar^+ laser model 2020 was used in the 514 nm mode for the excitation of the Raman light. Raman scatter was excited and collected through an Olympus BH microscope with an Olympus objective ($\times$100/NA = 0.95). A confocal microscope chamber was mounted in front of the spectrograph. The confocal chamber contained a variable-aperture pinhole placed in an image plane of the microscope. Continuous adjustment of the pinhole size between 50 and 1000 μm was possible without losing the accurate optical alignment. Unless stated otherwise, the pinhole diameter was set to 100 μm. The combination of an objective with $\times$100 magnification with a pinhole of 100 μm diameter gives rise to a lateral resolution of approximately 1 μm and a depth resolution on the order of 3 μm.[16,28] A two-dimensional, Peltier-cooled CCD camera (Wright Instruments) served for the detection of the Raman scatter. Care was taken to exclude

artifacts due to the influence of molecular orientation on the collected Raman scatter. The polarization effects of a weakly oriented sample material can usually be overcome by the use of circularly polarized excitation light. Hence, for all applications described here, a $\lambda/4$ plate was introduced in the laser beam to generate a circular polarization.

The instrument was used in the confocal laser line scanning mode, which permits the simultaneous collection of Raman spectra along a line of the sample.[29] For this, the angle under which the excitation laser beam enters the aperture of the microscope objective is modulated periodically using a first mirror scanner. This produces a single, focused spot on the sample which moves periodically along a line. Since there is a single illuminated spot scanning the sample, the collection of the Raman light can be made confocal by introducing a pinhole in an image plane of the microscope. A second scanner, operating synchronously with the first scanner, spreads the collected light into a line on the entrance slit of the spectrograph, thus preserving the spatial information of the collected Raman scatter. The spectrograph disperses the light of the illuminated line such that on a two-dimensional detector (usually a CCD), one dimension contains the spatial information of the sampled line while the other dimension contains the spectral information (see Fig. 1). The lateral spatial resolution along the line sampled is a function of the microscope objective, the wavelength of the light used for excitation, and the number and size of detector elements (pixels) the sampled line is imaged on. The CCD detector used here had 1152 by 298 detector elements. The long axis is used to collect the spectral information, while the spatial information is spread over the short axis. However, it is rarely necessary to have 298 distinct detector elements for the spatial information. To improve the signal-to-noise ratio, detector elements are commonly combined in the spatial dimension. Similarly, the detector elements in the spectral dimension can be combined if a high spectral resolution is not required. The larger detector elements resulting from spatial and spectral binning are denoted as Raman pixels.

The software allows the subsequent probing of lines on the sample, while the microscope table is moved stepwise in the direction perpendicular to the scanning direction of the probing laser beam. A predefined area can thus be mapped by collecting a rectangular array of sample points. The generated array containing a Raman spectrum for each sample point has to be processed to produce the desired image (i.e., the distribution of compound A in a second

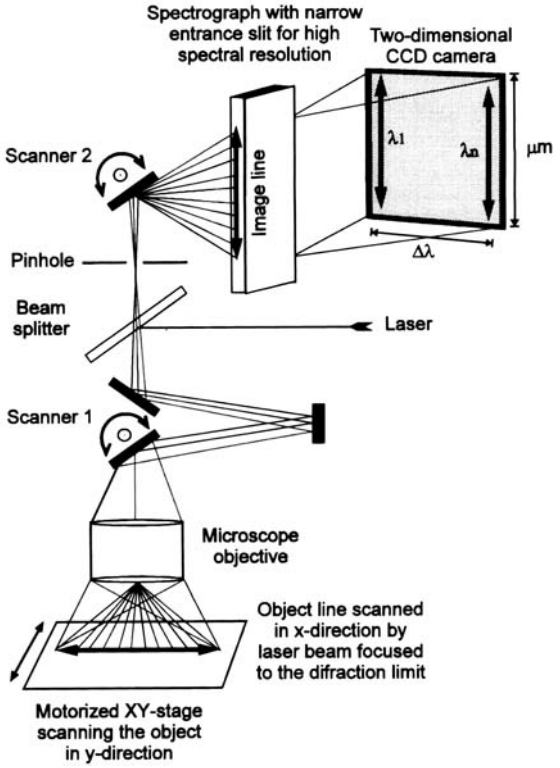

Figure 1 Schematic representation of Raman imaging by confocal laser line scanning using a point focused laser for the excitation of the Raman scattering.

compound B of a mixture of both). In a process of image arithmetic in which the area under a selected Raman band corresponding to compound A of the mixture is ratioed over the area under a Raman band corresponding to compound B of the mixture for all sample points of the array, an image is created which shows the distribution of the relative amounts of A and B in the sampled area. Since a Raman spectrum exists for each sample point, the full spectral information is available and other images containing details from different regions of the spectra can be generated at any later time.

By collecting the Raman scatter confocally, it is principally possible to produce optical sections at varying depth in translucent samples, which, with the appropriate software, can be manipulated to a three-dimensional representation of the original object. Similar three-dimensional imaging is already pursued in fluorescence microscopy.[30]

There are different modes of operation of this instrument (refer to Fig. 1). With scanner one and scanner two activated, the instrument acts as the laser line scanner described earlier. In case only scanner one is active and scanner two is set static, the instrument probes a line of the sample, but all

information is averaged into one spectrum. This is a convenient method to obtain average spectra of a sample containing inhomogeneities. Scanning the laser beam rapidly over the sample allows a better heat dissipation of the incident laser power. Higher laser powers can be used without burning the sample, thus reducing the collection time required for good signal-to-noise spectra significantly. For light-sensitive samples, this is often the only way to collect a Raman spectrum at all. The probing, low-power laser beam is scanned along a line while all scatter collected is binned together to form a good signal-to-noise average spectrum. Operating the system with both scanner one and two static corresponds to the ordinary, single-spot probing Raman microscope.

TRANSMISSION ELECTRON MICROSCOPY

To introduce sufficient contrast in the electron micrographs, the polymer samples were selectively stained. For this, the bulk samples were immersed in a 2% (w/v) aqueous solution of RuO_4 for 48 h. Since the staining medium penetrates preferentially into the amorphous phase, the crystalline regions appear as white structures in the micrograph.[31] A convenient side effect of the staining process is that the polymer hardens considerably and subsequent microtoming is facilitated. A Philips EM420T transmission electron microscope was used with an acceleration voltage of 120 kV.

APPLICATIONS

Ternary Polymer Blend: VLDPE/PBT/PC

Sample Description

The impact properties of polybutyleneterephthalate (PBT) can be improved by blending with very low density polyethene (VLDPE). Polycarbonate (PC) acts as a compatibilizer, since PBT and PC can chemically react in an esterification reaction to form a copolymer. The VLDPE is immiscible with both PBT and PC and hence forms a dispersed phase. The PC shows a weak tendency to encapsulate the VLDPE particles. Encapsulation of the VLDPE by the PC is found to reduce the surface tension of the PBT on the VLDPE segregated phase[2] and thus to improve the processability of the blend. All components are products of DSM, The Netherlands. Raman imaging is used to study the distribution of the different components within the sample.

The sample consists of a PBT matrix, with VLDPE and PC added as minor blend components. The components were coextruded in a miniextruder, and 5-μm-thick films were microtomed of the resulting blend. The sample proved to be extremely light sensitive, such that only very low laser powers could be used to excite the Raman scatter. The integration time had to be increased correspondingly to produce spectra of sufficient quality for a subsequent analysis. To capture more of the Raman scatter, the confocal pinhole was opened to 150 μm. Imaging of an area of 8 by 8 μm^2 was attempted with a resolution of four data points per μm. With a laser power of only 6 mW at the sample, the total time required for the collection of all Raman spectra with an acceptable signal-to-noise ratio increased to 8 h. At such long collection times, the stability of the microscope sample stage became a limiting factor for the image resolution. Only the top half of the image could be acquired before the sample film burned.

RESULTS

Figure 2 shows the transmission electron microscopy (TEM) picture of a thin section of the blend. Two phases can clearly be discerned from the matrix. One of the two segregated phases can also be seen to

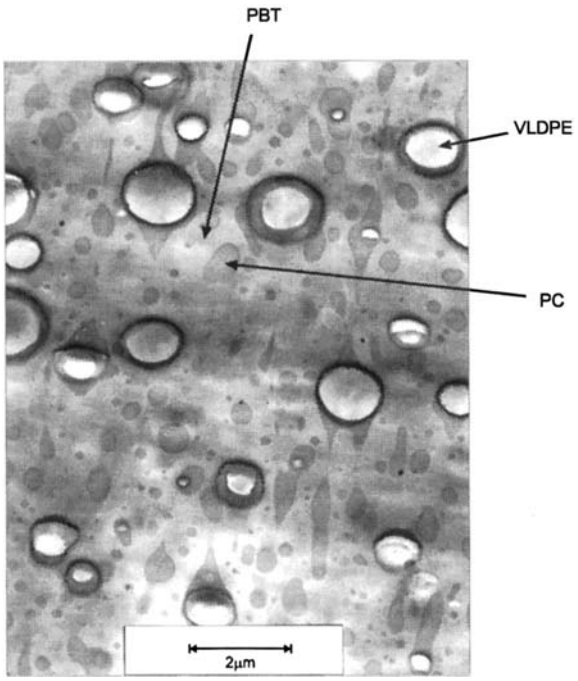

Figure 2 TEM micrograph of the ternary polymer blend sample of VLDPE, PBT and PC.

form envelopes around the other. Unfortunately, identification of the polymer materials by analysis of the crystalline lamellae structure is impossible. However, previous TEM analyses of binary blend systems of the aforementioned components permitted us to identify the matrix as the PBT and the distinct, round segregated phase as the VLDPE. The second dispersed phase and the encapsulating phase is thus thought to be the PC.

Figure 3 features the Raman spectra of the individual components of the blend. The Raman bands used for image construction are shown shaded. Almost all intense bands in any of the spectra coincide to some extent with a band in one of the other spectra. Three intense but highly overlapping bands have been selected to image VLDPE (approximately 1295 cm^{-1}), PC (1240 cm^{-1}), and PBT (1270 cm^{-1}). The high spectral resolution available with the confocal laser line scanning technique permits us to resolve the individual contributions from the spectrum of the mixture.

Figure 4(A) shows the Raman image obtained by ratioing the area under the Raman band at 1240 cm^{-1} over that at 1270 cm^{-1}. A dark shading corresponds to a high ratio and thus to a high content in PC with respect to PBT. During collection of the bottom half of the image, the sample burned and the spectra were featureless. Figure 4(B) shows a pseudo-3D representation of the image, and Figures 4(C) and 4(D) show the spectra extracted at locations corresponding to high and low Raman band area ratio, respectively. The spectra extracted are of sufficient quality, and the spectral features are well enough resolved for the identification of the individual components. The spectrum extracted at a high Raman band area ratio [Fig. 4(C)] is that of a mixture of mainly PBT with a minor contribution PC. No or only very little VLDPE contributes to the spectrum. The spectrum extracted at a low ratio contains PBT, a significant amount of VLDPE, and a small amount of PC.

An alternative image of the distribution of the Raman band area ratio (1295 cm^{-1}/1270 cm^{-1}) in the analyzed area was prepared for comparison (not shown here). It shows the distribution of the VLDPE phase in the PBT matrix. Comparing the two images of different Raman band ratios principally establishes that there are locations of segregated PC and VLDPE phase in the PBT matrix. No clear indication is present for the encapsulation of the VLDPE phase by PC as seen in the TEM micrograph. However, the encapsulating phase is generally of a thickness of a few hundred nanometres, too thin to be resolved properly by Raman microscopy. Furthermore, although the extracted spectra give evidence for a large variation in composition, the overall contrast in the images is low. This is due to the procedure used for the determination of the Raman band areas. The band areas are calculated as defined by the shading in Figure 3. For highly overlapping bands, this inevitably means that the calculated band area under one particular Raman band also contains contributions from its neighbouring bands. The spectral information is smeared out, and a decrease in contrast results. Proper curve-fitting analysis of the extracted spectra should enhance the contrast between the data points of the image significantly.

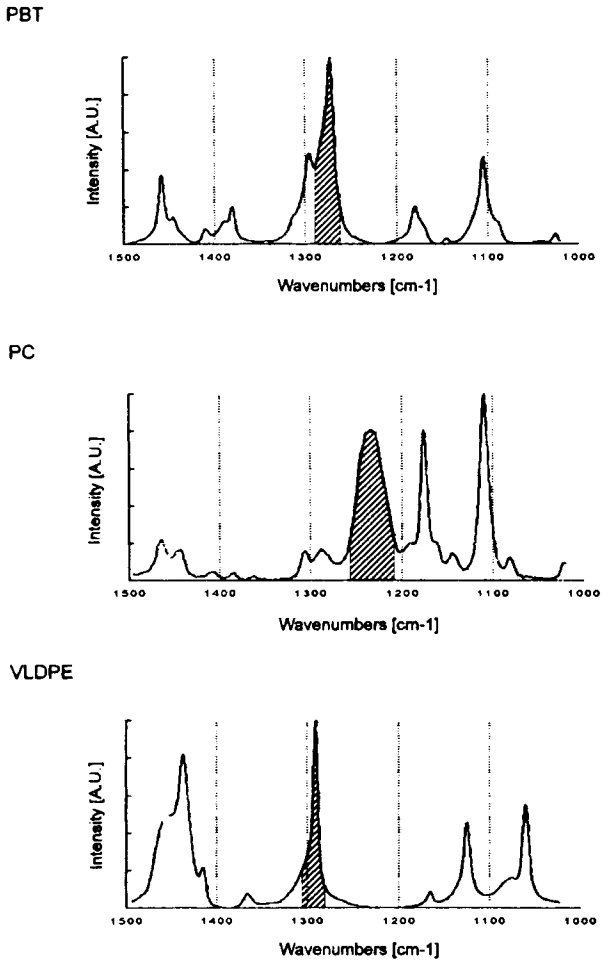

Figure 3 Individual Raman spectra of VLDPE, PBT, and PC. The Raman band areas used for construction of the Raman images are highlighted.

It is remarkable that independently of the position in the image, the extracted spectra indicate the presence of PBT. There is variation in the contribution of PBT to the spectra, but there seems to be not one location in the analyzed area which is free

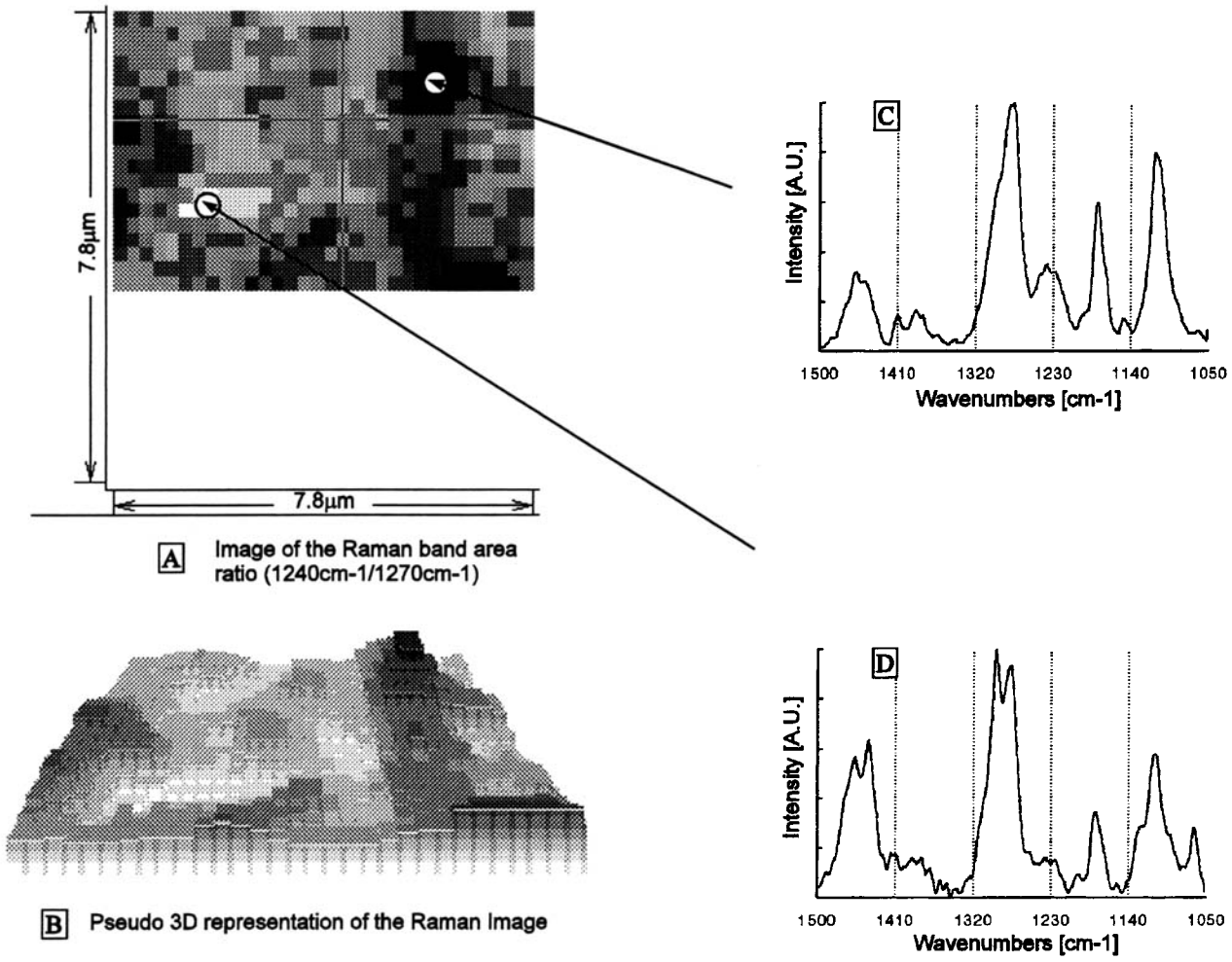

Figure 4 Raman imaging of the distribution of the individual blend components in a film of a ternary blend of VLDPE/PBT/PC. The image is based on the Raman band area ratio (1240 cm^{-1}/1270 cm^{-1}). A dark shading corresponds to a high ratio and thus to a high content in PC with respect to PBT.

from PBT. This is in contrast to the impression gained from the TEM micrograph, which shows two phases well separated from the matrix and points to an insufficient spatial resolution of the experimental setup. Because of the extremely low laser power that could be used, the confocal pinhole had to be opened to 150 μm diameter to collect more of the Raman scatter. Inevitably, this leads to a reduced depth and lateral spatial resolution, which manifests itself in the detection of Raman scatter from the surrounding matrix even at locations of segregated phase.

Principally, the experiment shows that it is possible to image the chemical composition of this particular blend. Locations of segregated phase rich in PC or VLDPE can be identified in the matrix of PBT. However, the light sensitivity of the sample prevented the acquisition of Raman spectra at adequate spatial resolution to allow a more detailed analysis. The image contrast may be increased by improved determination of the contribution of the different components to the extracted spectra.

Ternary Polymer Blend: SAN/SMA/PPO

Sample Description

For a miscibility study, a ternary polymer blend which consisted of two copolymers, 40% styrene-*co*-maleicanhydride (SMA—TU Dresden, containing 16% maleic acid anhydride) and 40% styrene-*co*-acrylonitrile (SAN—TU Dresden, containing 22.8% acrylonitrile) and one homopolymer 20% poly-2,6-dimethylphenylene oxide (PPO—GE Plastics) was produced. All three components were dissolved in toluene, and a film was cast onto a microscope glass

slide. After evaporation of the solvent, the blend hardened and a transparent film of about 10 μm thickness was obtained. The phase diagram for this mixture as obtained by DSC and cloud point measurements indicates the presence of three separate phases.[32] The size of the phase domains is anticipated to be on the order of 2–5 μm. Raman imaging of the component distribution should provide a convenient way to confirm phase separation, identify the composition of the different phases, and determine domain sizes.

Unlike in the study of the VLDPE/PBT/PC blend, the Raman bands of the single components selected for imaging were not overlapping (see Fig. 5). High spectral resolution was thus not a requirement. The Raman spectra were recorded on the Dilor XY800 system, but with a single 600 grooves/mm grating (approximately 10 cm^{-1} resolution). This setup allowed the coverage of the full spectral range of 4000 cm^{-1} in a single exposure of the CCD, so that the characteristic bands of all blend components could be measured simultaneously. A laser power of 25 mW at the sample could be used. An area of the sample of 16 by 16 μm^2 was analyzed with a data point pitching of 0.5 μm. The total collection time for the Raman image was 4 h.

Results

Figure 5 shows the spectra of the single components. Raman bands corresponding to CH stretching vibrations can be used to distinguish PPO from SAN and SMA. Both styrene-containing copolymers feature Raman bands at 2900 cm^{-1} corresponding to the stretching vibration of aliphatic CH groups and at 3050 cm^{-1} characteristic for aromatic CH stretching. PPO only contains aliphatic CH groups with a characteristic Raman band at approximately 2900 cm^{-1}. The spectra of SAN and SMA are essentially identical to that of styrene. Only the CN stretch vibration characteristic of the nitrile group in SAN at 2240 cm^{-1} allows a distinction.

The image in Figure 6(A) shows the distribution of the ratio of the Raman band at 3050 cm^{-1} over that at 2900 cm^{-1}. A dark shading represents a high ratio and thus a high content in SAN and SMA with respect to PPO. Figure 6(B) is the pseudo-3D representation of the image. SAN and SMA seem mainly to lodge in defined areas, separated from the PPO. However, while the spectrum extracted at a location of high ratio [Fig. 6(C)] indicates an almost pure styrene phase, the spectrum extracted at a low ratio [Fig. 6(D)] evidences PPO but also a significant amount of styrene.

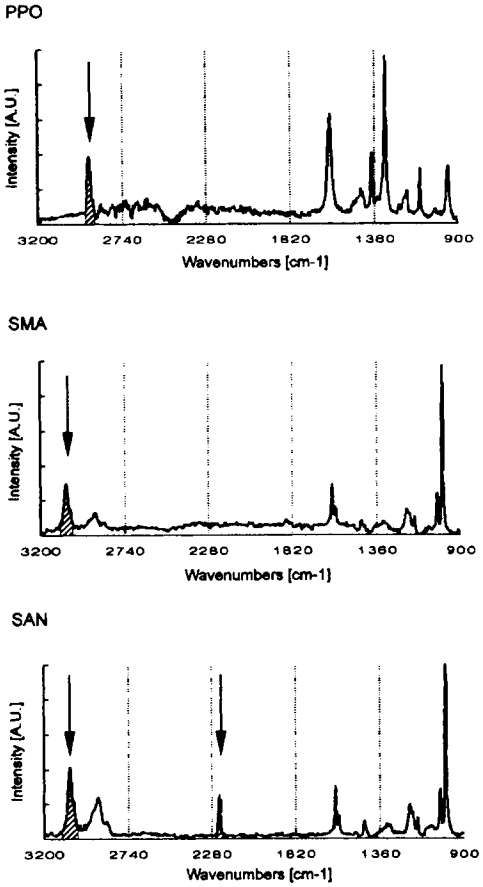

Figure 5 Individual Raman spectra of PPO, SMA, and SAN. The Raman band areas used for the construction of the conventional Raman images are highlighted.

Figures 7(A) and 7(B) show the image of the ratio of the area under the Raman band at 2240 cm^{-1} over that at 2900 cm^{-1} and the corresponding pseudo-3D representation. The dark shading stands for a high ratio and thus for a high content in SAN with respect to PPO. The images are essentially comparable to those in Figure 6(A) and 6(B) in number and shape of the features. However, a direct comparison of the images in Figures 6(A) and 6(B) with those in Figures 7(A) and 7(B) gives evidence for phase separation of the SAN and SMA phase. While the features in the foreground on the left-hand side of Figures 6(A) and 6(B) seem to contain mainly SMA, those at the far end appear to contain mainly SAN.

Three separated phases can thus be discerned. A continuous PPO/SAN/SMA phase is present in the major part of the analyzed area with interspersed discrete phases of high SAN/low SMA and of high SMA/low SAN content. The SAN/SMA forms regions free from PPO of a size on the order of 3–7 μm diameter.

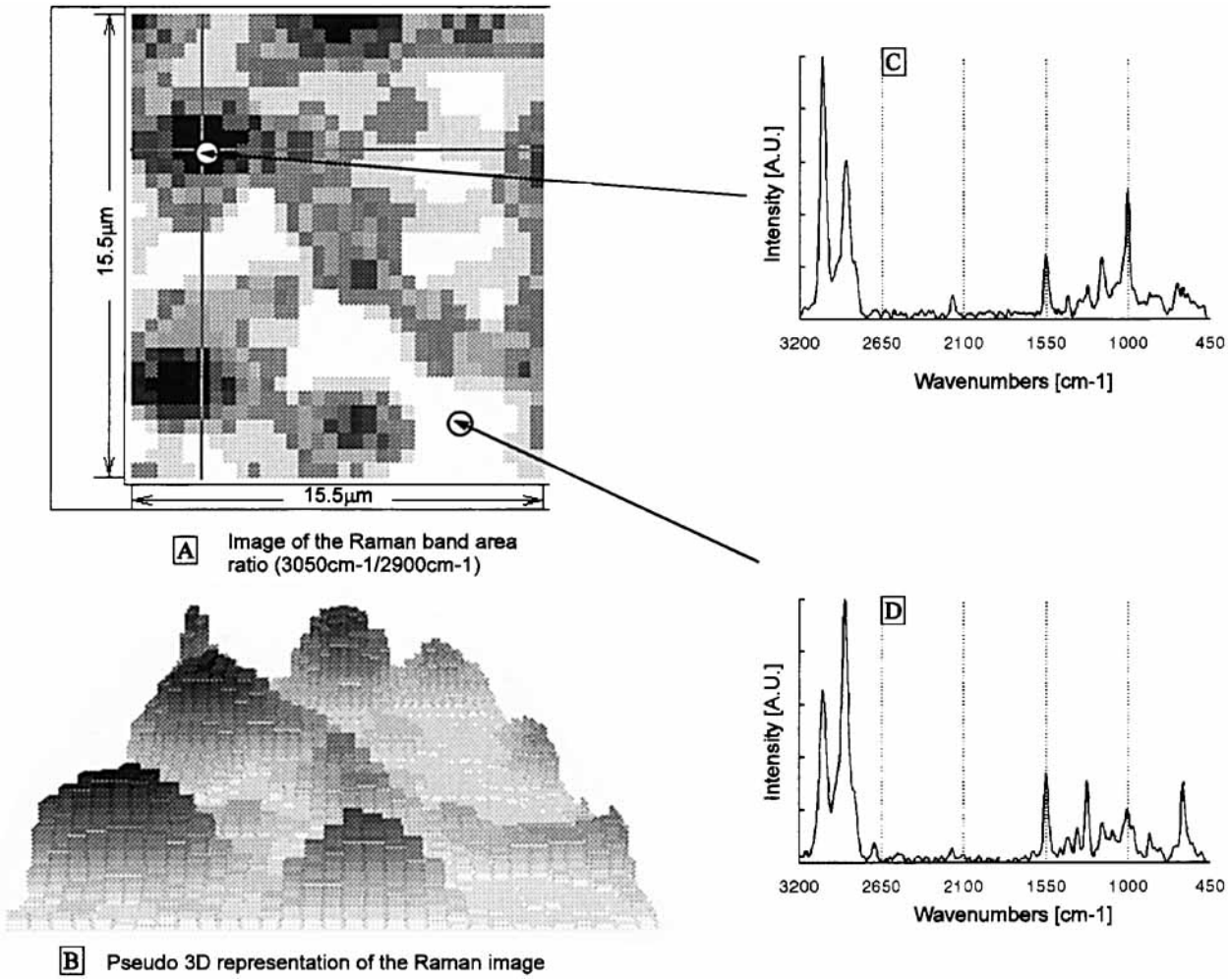

Figure 6 Raman imaging of the distribution of the individual blend components in a film of a ternary blend of PPO/SAN/SMA. The image is based on the Raman band area ratio (3050 /2900 cm^{-1}). A dark shading corresponds to a high ratio and thus to a high content in SAN and SMA with respect to PPO.

Optical Fiber Preform Based on a Blend of Two Different Polyacrylates

Sample Description

For short data transfer lengths where absorption losses are of little relevance (typically 10–100 m), it is interesting to develop optical fibers based solely on organic polymers since they are cheap and offer a comparatively high flexibility and insensitivity to mechanical load.

To retain light in an optical fiber, it is necessary to produce an index profile in which the fiber core material is of higher refractive index than the cladding. In the most simple form, this is achieved with a stepped index profile. Higher data transfer rates can be achieved with continuously graded index profiles (GRIN). In case of polymer optical fibers, a monomer, which yields a high refractive index core once it is polymerized, is placed in the centre of a fiber preform of a polymer with low refractive index. Diffusion of the monomer from the core into the cladding polymer can be induced thermally, establishing a concentration profile. The diffusion process is stopped by polymerization of the monomer. A refractive index profile is obtained which parallels that of the composition. In a subsequent step, the fiber preform is drawn into fiber-optic cable, retaining the refractive index profile of the preform. For the optimization of the production method for fiber preforms, the preforms need to be tested frequently for their refractive index profile. Currently, this is done with interference microscopy, requiring the sample to be cut in thin slices.[33] The technique is simple but time consuming. Raman imaging of the com-

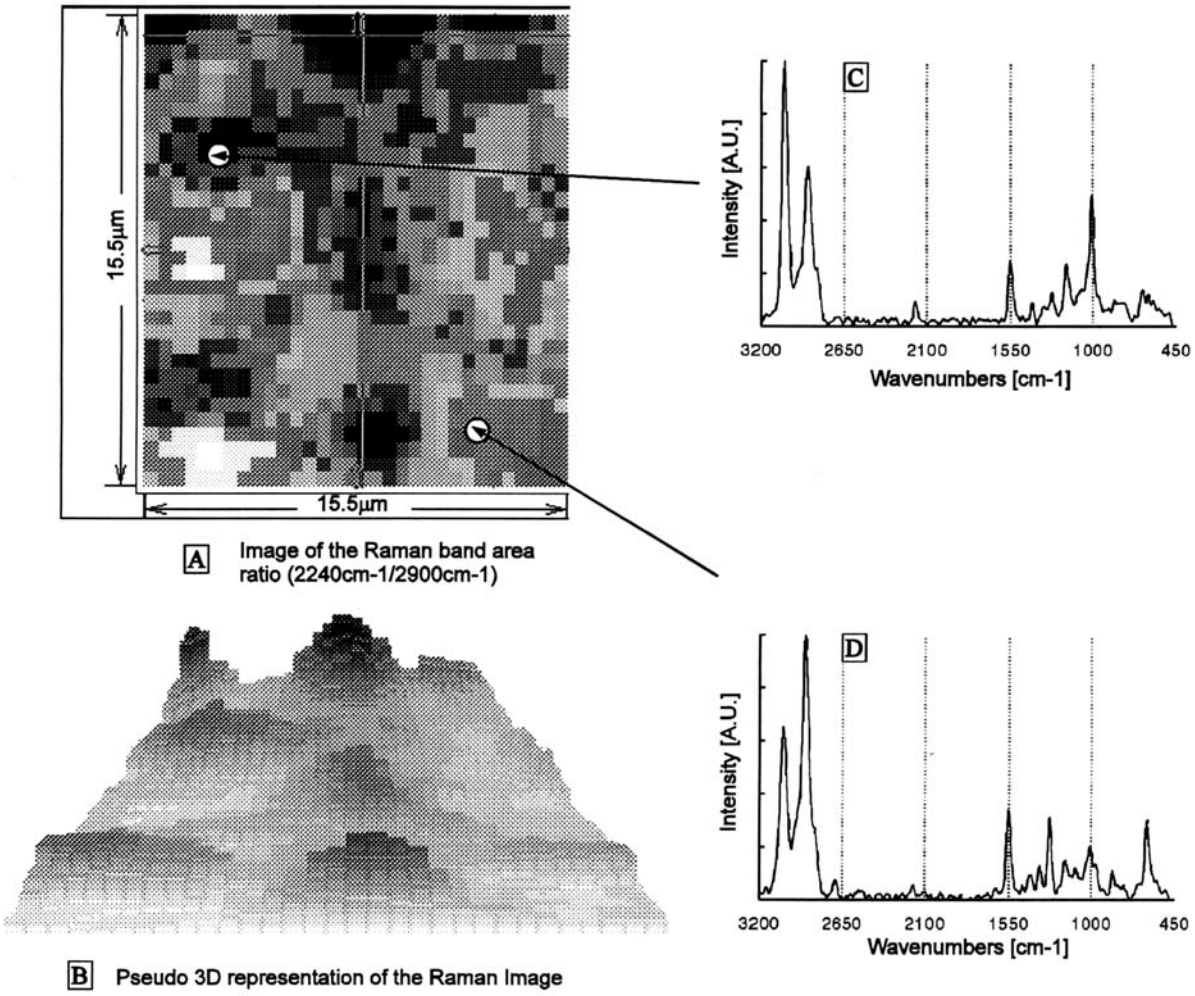

Figure 7 Raman image as in Figure 6 but based on the Raman band area ratio (2240 cm^{-1}/2900 cm^{-1}). A dark shading corresponds to a high ratio and thus to a high content in SAN with respect to PPO.

position of cladding and core should provide comparable information without having to pretreat and damage the sample.[34]

The sample used in this study consists of a fiber preform in the shape of a cylinder of 18 mm diameter. Both cladding and core material are based on acrylate monomers. For the cladding, however, a chemically modified acrylate monomer was used which yields a lower refractive index in the polymerized state. A fiber preform was produced by filling a cylindrical mould with the cladding monomer, which was then fully polymerized. Subsequently, a hole was drilled in the center of the preform and filled with the core monomer. Before thermally induced polymerization, the core monomer was given time to diffuse at elevated temperature into the cladding polymer.

For the Raman imaging, the scanner was set to scan a line of approximately 8 μm length in a direction perpendicular to the fiber preform radius. The detector elements were grouped together to form two larger detection elements, averaging 4 μm length of the scanned line each. The y stage was set to move the scanned line in steps of 50 μm along the radius from the outer cladding to the center core of the fiber preform. The scanned rectangular area had a dimension of 8 μm width and 9000 μm length. A high laser power of 90 mW at the sample could be used, which reduced the collection time for spectra with good signal-to-noise ratio to 20 s. The total

time required for the collection of all spectra amounted to 1 h.

Results

The pure component spectra of cladding and core material are shown in Figure 8. The Raman spectra of core and cladding polymer are significantly distinct from each other. The Raman band at 813 cm^{-1} only appears in the spectrum of the core polymer, while the Raman band at 603 cm^{-1} appears in both core and cladding spectra at approximately identical intensity. The Raman band area ratio (813 cm^{-1}/603 cm^{-1}) is thus directly proportional to the concentration of the core polymer. Figure 9 shows the concentration of the core polymer as extracted from the scanned area along two lines reaching from the outer cladding (0 μm) to the inner core (9000 μm) of the fiber preform. The concentration profiles rise in two drawn-out steps from the outer cladding to the inner core. This profile should closely resemble the refractive index profile of the fiber preform. It is obvious that the aim of producing a stepless, graded index profile in the fiber preform has not been achieved in this sample. The spatial resolution of the Raman microscope is sufficient to perform a similar analysis on the drawn fiber. For further studies, a set of calibration standards of known composition could be analyzed such that the measured core polymer concentration in the core/cladding transition region can be converted into refractive index numbers.

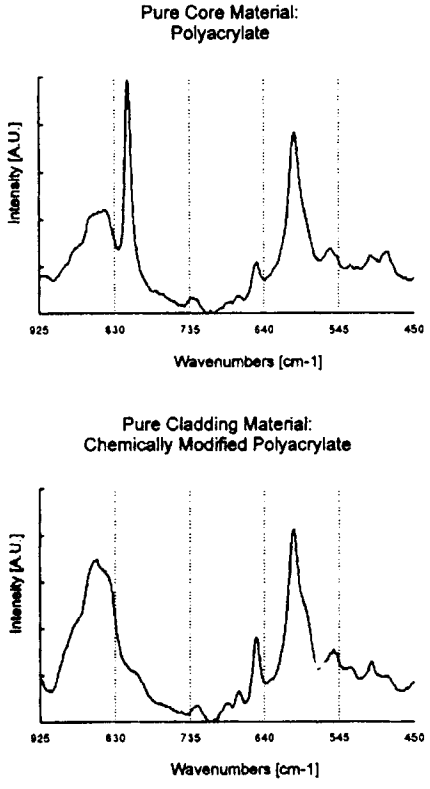

Figure 8 Individual Raman spectra of the different polyacrylates used for the fabrication of the fiber preform.

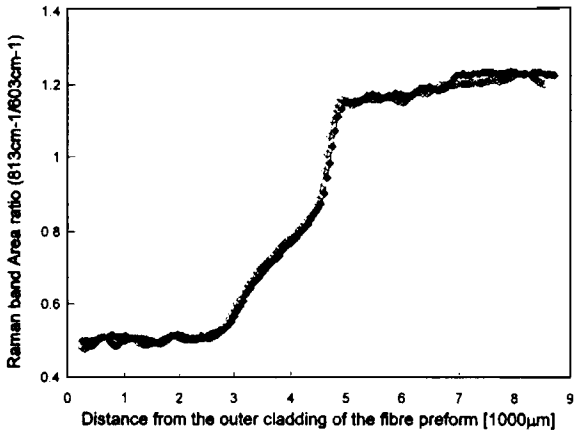

Figure 9 Profiles of the ratio of the area under the Raman band at 813 cm^{-1} over that at 603 cm^{-1}. The profiles were extracted along a line from the outer cladding (position 0 μm) to the inner core (position 9000 μm) of the fiber preform. See text for details.

Melamine–Formaldehyde Resin

Sample Description

Melamine–formaldehyde (MF) resins are thermosetting materials used in decorative laminates. Systematic research on MF resins is aiming toward improving their material properties. It was tried to lower the formaldehyde to melamine ratio (F/M), resulting in a lower concentration of networking bridges in the three-dimensional network structure. This may result in the presence of melamine, which is not bonded to formaldehyde. This might have consequences for the network structure, the shelf life of the resins, and the mechanical properties of the cured resin.

In recent publications, the use of Raman spectroscopy for the characterization of MF resins was reported.[35,36] It could be shown that Raman spectroscopy can be used to study the methylolation and network formation reactions between melamine and formaldehyde.[35] The content of free melamine in cured MF resins can be determined by analyzing the Raman band intensity ratio of the bands at 676 cm^{-1} and 975 cm^{-1}, which are due to vibrations in the triazine ring of the melamine.[36] The band at 676 cm^{-1} is only present in free, unreacted melamine,

whereas the band at 975 cm^{-1} is present in the free melamine as well as in the different substituted forms.

Raman imaging is used to study the distribution of free melamine in a cured MF resin sample. The model sample consisted of a MF plate with a non-commercial F/M ratio of 0.9 obtained by mixing a resin of F/M ratio of 1.7 with free melamine and subsequent curing under pressure. An area of 44 by 44 μm^2 was divided into 12 by 12 Raman pixels, each pixel representing an area of 3.7 by 3.7 μm^2. The acquisition time for the total image amounted to approximately 10 min using a laser power of about 25 mW at the sample.

Results

Under the illumination with laser light for the excitation of the Raman scatter, the melamine–formaldehyde sample gave rise to a considerable fluorescence signal. The Raman signal was still discernable from the strong fluorescence background. However, the background intensity was so high that the time for the collection of the Raman spectra had to be limited to prevent the saturation of the CCD detector. Hence, only a limited signal-to-noise ratio could be obtained in the Raman spectra. Still, the spectra were of sufficient quality to allow the Raman imaging of the distribution of free melamine in a cured melamine–formaldehyde sample. Figures 10(A) 10(B) show the Raman image and the corresponding pseudo-3D representation of the ratio of the Raman band at 676 cm^{-1} over that at 975 cm^{-1}. A dark shading corresponds to a high ratio and thus to a high content in free melamine. Figures 10(C) and 10(E) show the spectra extracted at locations of high and low free melamine content, respectively. The profile in Figure 10(D) was extracted along a line as indicated in the image. The results obtained for this particular sample show that the sample composition is very inhomogeneous. Regions of high free melamine content of about 10 μm in diameter can be identified in a matrix of low free melamine content.

Distribution of a Foaming Agent in a Polypropene/Polyethene Blend Foil

Sample Description

Foamed polymers are of significant commercial importance in applications such as thermal insulation, protective packaging, and the sealing of beverage containers. Depending on the type of application, vastly different methods of preparation are used. A common way to produce thin films of foamed polymer involves the addition of a foaming agent in a compounding step. When exposed to a well-defined temperature, this compound disintegrates, thereby releasing an inert gas. The released gases are captured as bubbles in the viscous matrix polymer melt. The mechanical characteristics of the final foam are determined by the size and the amount of the cavities. These, in turn, are related to the concentration and the distribution of the foaming agent in the compounded polymer films before the actual foaming step. To control the foaming step, it is desirable to analyze the homogeneity of the distribution of the foaming agent in the compounded films.

The sample analyzed here consisted of a thin tile of approximately 0.5 mm thickness of a blend of polyethene with polypropene. Azobiscarbonamide was added as foaming agent, releasing nitrogen upon thermal treatment. An area of 122 by 162 μm^2 was analyzed with 20 by 20 data points, each data point corresponding to a size of 6 by 8 μm^2. With a laser power at the sample of 80 mW, the total collection time of the image amounted to approximately 2 h.

Results

The Raman image of the distribution of the foaming agent in the polymer matrix is shown in Figure 11(A). For this, the ratio of the areas under the Raman band at 1570 cm^{-1} (Azobiscarbonamide) over that at 1460 cm^{-1} (polypropene and polyethene) is used. A dark shading relates to a high ratio and hence a high concentration of the foaming agent. Figure 11(B) shows the corresponding pseudo-3D image. The spectra extracted at locations of a low and a high ratio are shown in Figures 11(C) and 11(D), respectively. Spectrum C is that of the pure polyethene/polypropene blend without any contribution of the foaming agent. Spectrum D is that of the pure foaming agent. From the Raman imaging analysis, it becomes clear that the foaming agent is very inhomogeneously distributed in the polymer matrix forming isolated particles of approximately 15–20 μm diameter.

PE–Epoxide Composite

Sample Description

In fiber composite samples, one of the dominant characteristics determining material properties is the stress transfer from the fibers to the matrix material. In previous studies, confocal Raman microscopy was used for the point analysis of the local stress transfer between fiber and matrix.[16,37] For this

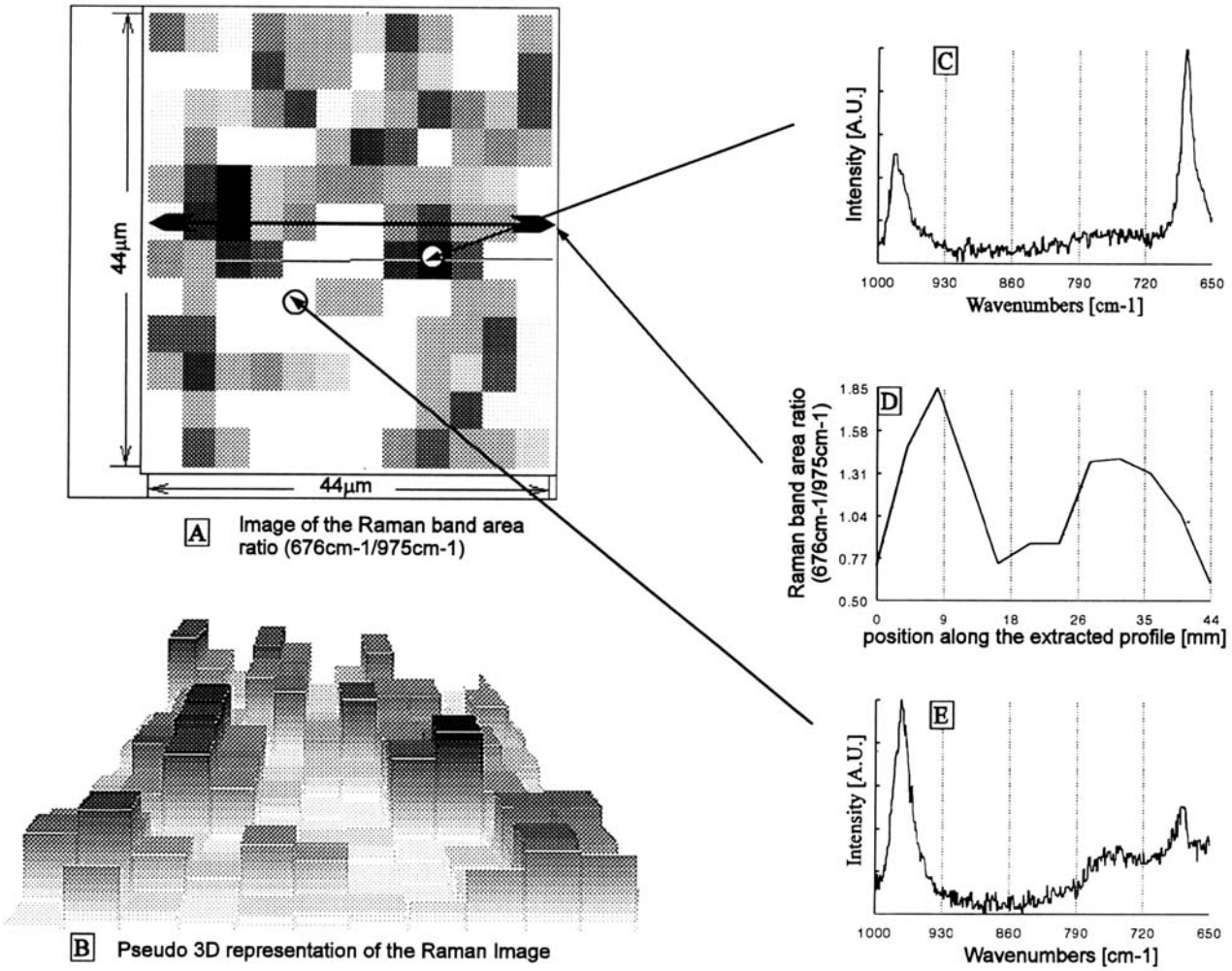

Figure 10 Raman imaging of the distribution of free melamine in a bulk sample of melamine–formaldehyde. The image is based on the Raman band area ratio (676 cm^{-1}/975 cm^{-1}). A dark shading corresponds to a high ratio and thus to a high concentration of free melamine.

purpose, a model composite was prepared, consisting of a high E-modulus polyethene fiber (Dyneema SK60, approximate diameter 15 μm from DSM, The Netherlands) embedded in an epoxy layer (XB5082 with XB5083 hardener from Ciba Geigy) with a thickness of 100 μm. Raman imaging by confocal laser line scanning is used to analyze the sample structure, with the polyethene fiber immersed several tens of micrometres into the matrix material. For Raman imaging, an area of 34 μm by 38 μm was selected such that a section of the fiber and the adjacent matrix material were included. Grouping of the CCD in the spatial direction was performed to form 10 Raman pixels with a width of 3.4 μm each, yielding the total length of 34 μm approximately parallel to the length of the polyethene fiber. In the perpendicular direction, the stepping motor of the microscope stage was moved in 30 steps of 1.25 μm to cover the total length of 38 μm. The laser power at the sample was 10 mW. The collection time per single sample point was 3 s, such that the total collection time of the image amounted to 15 min.

Results

Figure 12(A) features a white light TV image of an area of the composite. The structure of the fiber can be distinguished from the matrix epoxide. For better recognition, the fiber is highlighted using dashed white lines. Within the fiber, the microfilaments can be discerned by the lines along the direction of the fiber. The Raman image was constructed calculating the Raman band area ratio of the bands at 1060 cm^{-1} due to the polyethene fiber over that at 1180

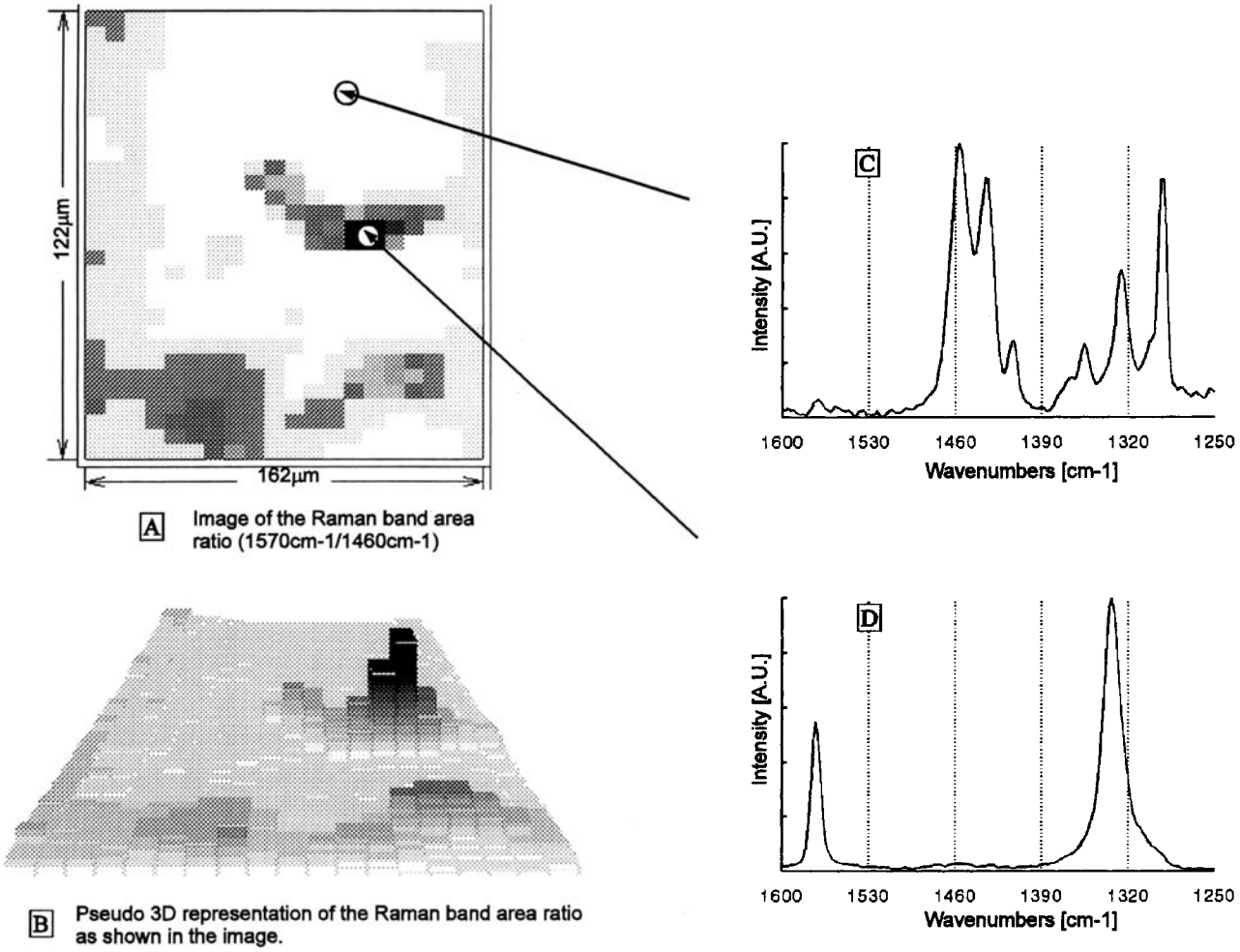

Figure 11 Raman imaging of the distribution of a foaming agent in a compounded bulk polyethene/polypropene blend sample. The image is based on the Raman band area ratio (1570 cm^{-1}/1460 cm^{-1}). A dark shading corresponds to a high ratio and thus to a high content in foaming agent with respect to the blend matrix.

cm^{-1} due to the epoxide matrix material. The Raman band areas were taken as defined in the spectra of the pure components (Fig. 13).

From the 2D image presentation in Figure 12(B), the shape of the fiber can be clearly recognized. The fiber and the matrix featured a large difference in fluorescence background. It was possible, though, to remove the influence of the fluorescence by computerized subtraction of the background from the individual spectra in the spectral image. Spectra extracted at a position of high (in the middle of the fiber) and low Raman band area ratio (in the matrix) are shown in Figures 12(E) and 12(D), respectively. These spectra compare well with those taken of the pure components (Fig. 13). Taking into account that the polyethene fiber is immersed into the epoxide layer by about 40 µm, the Raman spectroscopic distinction between fiber and epoxide matrix is excellent. A profile of the (1060 cm^{-1}/1180 cm^{-1}) Raman band area ratio extracted along a line across the fiber, as indicated in the image, is shown in Figure 12(C). The profile is unexpected for a fiber which was thought to be circular in shape. It turned out, however, that the polyethene fibers used in the sample were of what is commonly called "bean shape," a fact that matches the observed profile. Figure 14 shows the pseudo-3D representation of the Raman band intensity ratio distribution in the imaged area. Also here, the bean shape of the fiber can be recognized. Hence, confocal Raman imaging using point focused illumination is able to image polyethene fibers immersed in a matrix of epoxide. The ability of the confocal arrangement to suppress a large part of the fluorescence originating from ma-

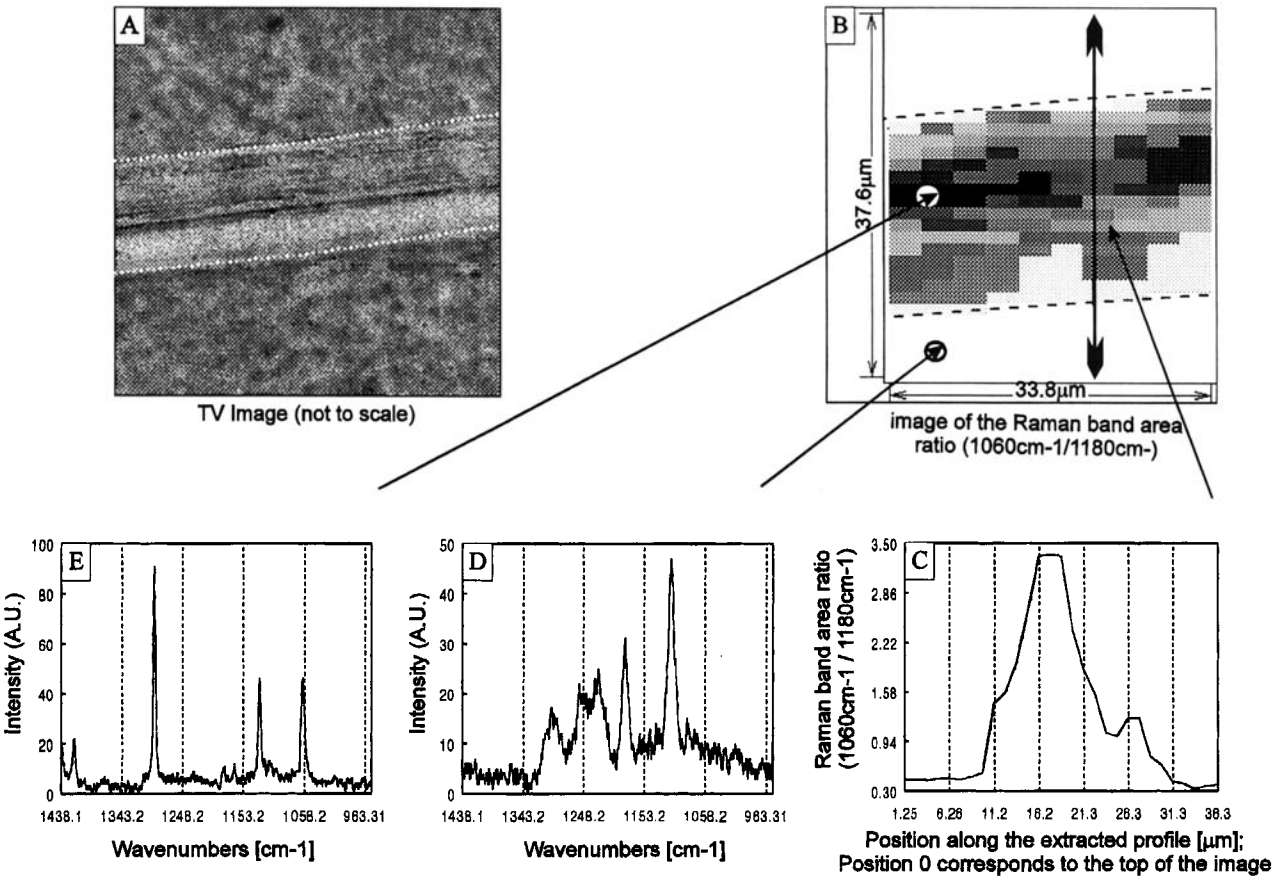

Figure 12 Raman imaging of a polyethene fiber/epoxide composite by point illumination and confocal light collection. See text for details.

terial adjacent to the probed volume plus the possibility to treat all spectra individually before the formation of the image alleviate the problem of sample fluorescence to such an extent that excellent images can be obtained.

The ability of the confocal arrangement to suppress a large part of the Raman scatter and fluorescence originating from material adjacent to the probed volume permits the collection of images with high contrast. Principally, it should be possible to apply Raman imaging to the efficient mapping of stress distribution in composite materials.

Ternary Polymer Blend: PP/PE/EPM

Introduction

Commercial isotactic polypropene homopolymer is limited in its applications by its relatively low impact strength and high brittleness temperature. The impact properties of the polymer can be greatly improved by blending with a minor fraction of a rubberlike ethene–propene random copolymer while maintaining stiffness, strength, thermal stability, and processability at a desired level.[38] Blends of polypropene with ethene–propene random copolymers (and polyethene) are generally known as high-impact polypropene and dominate a large fraction of the polypropene market. High-impact polypropene can be prepared by physically blending the individual components and performing subsequent coextrusion. The components of impact polypropene are found to be phase segregated such that sample inhomogeneities arise on a microscopic scale.[39] Polypropene and polyethene are assumed to be incompatible. The random copolymer contains segments of both polyethene and polypropene and is thought to locate preferentially between the two homopolymers. A shell of copolymer forms around the segregated homopolymer and effectively separates it from the matrix.[40] In this way, it acts as a compatibiliser between the homopolymers. More recently, the possibility of a diffusion of the copolymer material into the amorphous phase of the homopolymers has been discussed.[41] Raman imaging is applied to the characterization of the compositional and

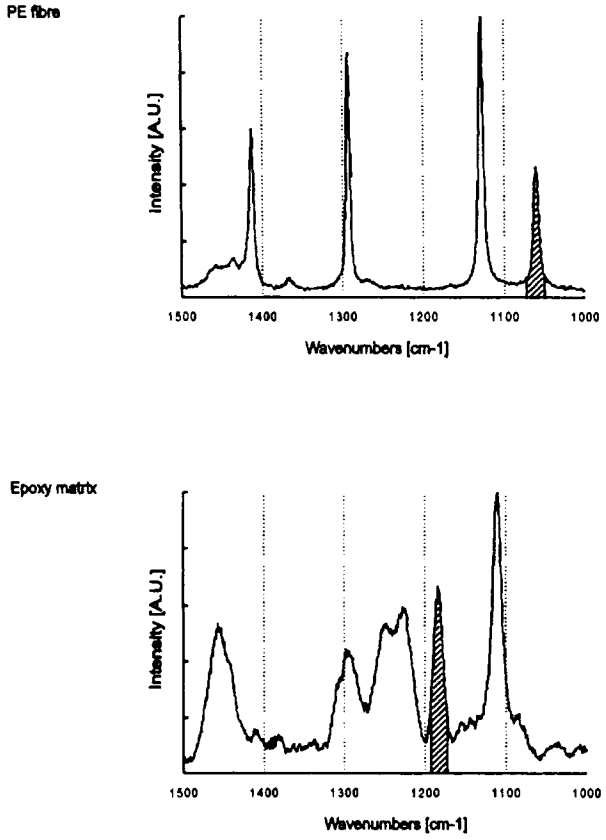

Figure 13 Individual Raman spectra of the pure components polyethene fiber and epoxide matrix used in the composite sample. The Raman band areas used for image construction are highlighted.

morphological structure in a physical blend of polypropene, polyethene, and an ethene–propene copolymer of narrow composition distribution. For the imaging of the samples, a careful selection of the most promising Raman bands had to be made.

Imaging of Polypropene in Blends with Ethene-Containing Polymers

The typical room temperatures Raman spectra of polyethene, isotactic polypropene, and an ethene–propene random copolymer of 70/30 percentage monomer composition are shown in Figure 15. For the imaging of polypropene-rich regions in blends with ethene-containing polymers, the ratio of the area under the Raman band at 1330 cm^{-1} (polypropene exclusively) over that under the Raman band cluster at 1296 + 1305 cm^{-1} (ethene-containing polymer: polyethene and ethene–propene copolymer) was used.

Random Ethene–Propene Copolymer

The spectrum of the copolymer resembles that of a mixture of amorphous polypropene with amorphous polyethene. There are no characteristic copolymer Raman bands significantly distinct from those of semicrystalline polyethene or polypropene homopolymer. A Raman spectroscopic separation of the copolymer from a blend with polypropene and polyethene by single band fitting appears impossible. However, the copolymer has a spectrum of characteristic shape, and the determination of the copolymer contribution to the overall blend could be attempted by weighted curve fitting. For this, an extended spectral range of the individual blend component spectra is fitted into the spectrum of a

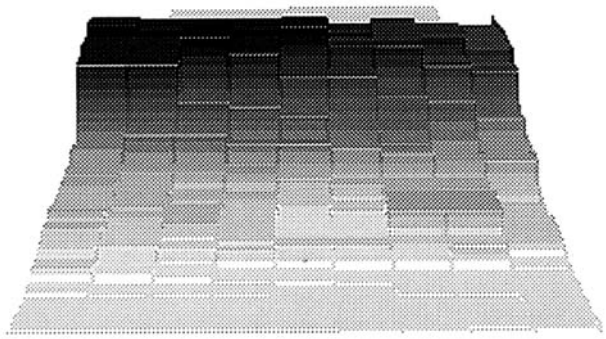

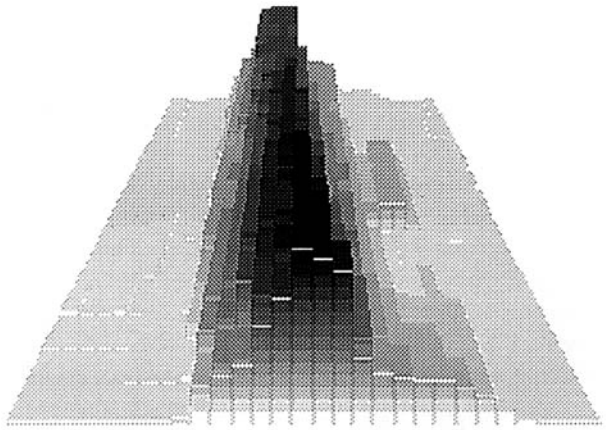

Figure 14 Pseudo-3D representation of the distribution of the Raman band area ratio (1060 cm^{-1}/1180 cm^{-1}) in the imaged area around a polyethene fiber in a matrix of epoxide.

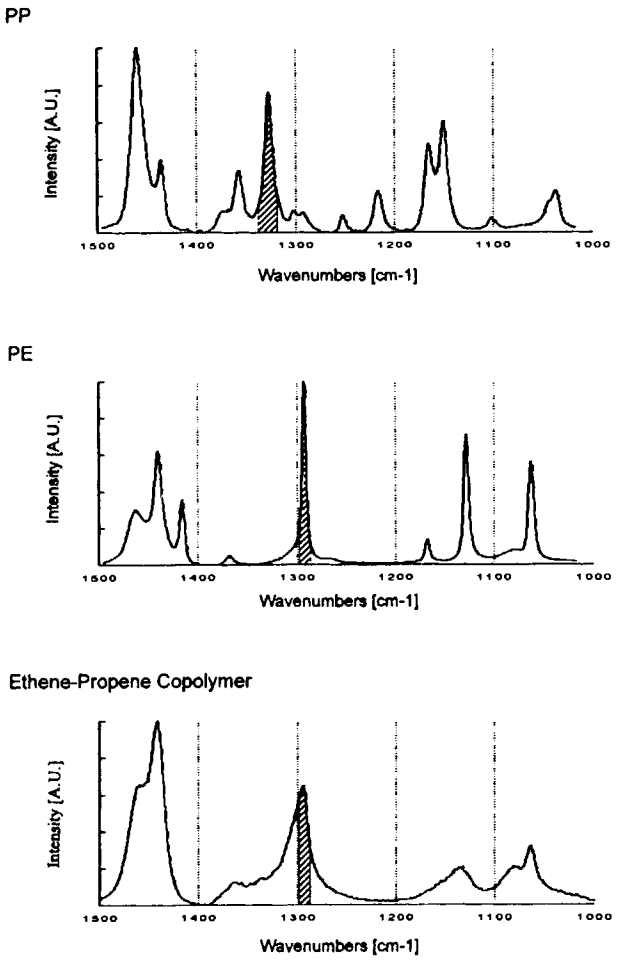

Figure 15 Schematic representation of the Raman spectra of the different components used in the blends. The Raman band areas used for the construction of the rough composition images are highlighted.

blend of unknown composition. Prerequisite for weighted fitting is that the spectra of the individual components do not change upon mixing. For this, the components must not interact with each other such that mixing on a molecular scale leads to significant changes in relative band intensities and/or positions.[42] Neither of the components of the blends analyzed here contains polar groups, and a strong chemical interaction is not expected. However, differences in polymer crystallinity and orientation will affect the quality of the fit. Consequently, the spectral regions which show strong variation with crystallinity and molecular orientation should be excluded as far as possible. The spectral region between 1400 and 1250 cm^{-1} was empirically determined to be most suitable for the separation and quantification of the three components of the high-impact polypropene blend by weighted curve fitting.

Crystallinity in Semicrystalline Polypropene

The choice of Raman bands for the determination of crystallinity in polypropene is quite difficult. In isotactic polypropene, the chains preferentially arrange in a regular helical structure[43,44] and do not interact with each other in a way that gives rise to crystal field splitting. Hence, there are no Raman bands which can directly be related to the crystalline state. Nevertheless, a number of publications have appeared on the use of Raman spectroscopy for the determination of crystallinity in polypropene samples.[45–48] Essentially, these are based on the detection of the relative amount of structurally perfect helices in the polymer. Although not necessarily correlating with polypropene crystallinity, stretches of perfect helix structure are a prerequisite for the formation of regular aggregates of chains in larger crystalline structures. The Raman band area ratio (1167 cm^{-1}/1152 cm^{-1}) was used here to estimate the polypropene crystallinity. The conversion of the Raman data into percentages of crystallinity could be attempted by establishment of a calibration curve. However, to obtain a picture of the homogeneity of the crystallinity across mold injection plates, comparison of the spectroscopic data appeared sufficient.

Experimental

Samples and Sample Preparation. The high-impact polypropene sample was prepared by blending polypropene (Stamylan P 13E10, DSM) with polyethene (Stamylan HD 7625, DSM) and an ethene–propene copolymer with 70/30 ethene-to-propene ratio (Tafmer, DSM) to give a final composition of 78% polypropene, 14.5% polyethene, and 7.5% copolymer. The routine used for weighted curve fitting was calibrated using a range of binary polyethene/polypropene blends of known composition. For all blends, the components were mixed as granulate, extruded, and injected into a mold. To reduce variation in polymer crystallinity related to the processing conditions, all samples were produced with a similar thermal history. Principally, the depth resolution of the confocal Raman microscope permits us to study the samples in the bulk form.[28] However, from transmission electron microscopy of the high-impact polypropene blend, it is known that the diameter of the dispersed phase is of the order of 1 μm. This is at the bottom range of the resolving power of the microscope such that the maximum possible spatial resolution has to be used. The depth resolution of the confocal Raman microscope is on the order of 2–3 μm, though sample material farther

away from the focal plane does also contribute to a small extent to the Raman spectrum (see ref. 28 and references therein). To overcome uncertainties in the Raman image due to the depth resolution, films of 2 μm thickness were prepared from the blend samples by microtoming at liquid nitrogen temperature.

Curve-Fitting Analysis. Two principally distinct curve fitting procedures were used. To extract the relative composition of a blend consisting of polypropene, polyethene, and a ethene–propene copolymer, a curve-fitting routine was developed which allowed the weighted fitting of a complete spectral range of the individual component spectra into spectra recorded from a blend of the components. The program is based on the linear addition of the individual component spectra (A, B, and C) plus a background into an unknown total spectrum (T) according to

$$T = (y \cdot A) + (x \cdot B) + (z \cdot C) + \text{Background}$$

The fitting result is presented in relative amounts of component A (polypropene), B (polyethene), and C (ethene–propene copolymer) in percent.

The individual component spectra used for the fitting were obtained by averaging a large number of spectra recorded from an area on the respective sample to avoid artifacts due to local inhomogeneities in morphology. Furthermore, the focal plane of the confocal microscope was immersed several micrometers under the sample surface to exclude surface effects.

The curve-fitting routine proved extremely sensitive to small shifts in peak position. Such shifts occur when the ambient temperature of the spectrometer is not controlled accurately. Since the collection time required for the large number of spectra forming a Raman image of high spatial resolution sometimes amounted to several hours, it occurred that the peak positions in the spectra recorded first differ from those recorded last. The spectra of the pure, individual components were therefore taken in quick succession and under identical conditions. The peak positions in the individual component spectra were then fixed with respect to each other. For the weighted fitting of the unknown blend spectra, the set of individual component spectra was allowed to shift freely but unanimously in direction and extent on the wave-number axis within a limited bandwidth of 1.5 cm^{-1}. This bandwidth proved excessive since the maximal bandshift required to obtain good fits never exceeded 0.7 cm^{-1}. Without any further correction, the composition of the binary calibration blends as derived by weighted fitting approached the actual composition closely. The method was refined by adjusting the relative spectral weight of the individual component spectra. For the ultimate test, the weighted fitting routine was applied to determine the composition of average spectra obtained from ternary blends of polyethene, polypropene, and ethene–propene copolymer of known composition. The blend composition could be determined with an accuracy of 5–10%.

An entirely different method of curve fitting was used for the analysis of polypropene crystallinity. The determination of Raman band areas was done by fitting of single peaks into clusters of Raman bands using the GRAMS software from Galactic Industries. Voigt profiles were assumed for the shape of the Raman bands.[49]

Results and Discussion

Blend Morphology. Figure 16 shows a transmission electron micrograph of the blend. In a continuous matrix, segregated particles of a wide size distribution can be seen. The particles are elongated in the direction of mold injection, and the particle size ranges between a few tenths of a micron to several microns. The staining medium, which had been used to prepare the samples for the electron microscopical analysis, penetrates preferentially into the amorphous phase of the different blend components. Consequently, the crystalline regions of the blend are not or less stained and appear white in the micrograph. Besides the heavily stained, black regions corresponding to amorphous polymer, two distinct lamellar structures can be identified. The cross-hatched lamellae is typical for regions with polypropene as the predominant crystalline species. Regions of predominantly crystalline polyethene can be detected by its typical fibrillous lamellae (see markers in Fig. 17).[31] The picture shows segregated, particle-like regions of high polyethene content surrounded by amorphous material, which is supposedly the copolymer phase. The segregated phase is embedded in a matrix of high polypropene content. Hence, from the transmission electron micrographs it is possible to determine the general morphology of high-impact polypropene blends and to detect the preponderant crystalline species at a sampling location. However, information about the minor crystalline components cannot be extracted. The composition of the amorphous regions is inaccessible. Furthermore, it is impossible to extract any infor-

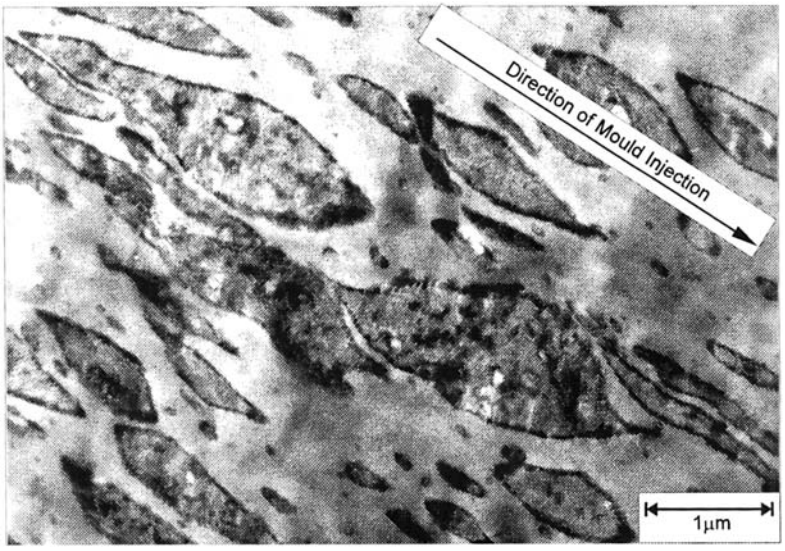

Figure 16 TEM micrograph of sample *A*: 14.5% polyethene/7.5% ethene–propene random copolymer/78% polypropene.

mation on the degree of crystallinity of the constituents.

Raman Analysis at High Spatial Resolution. For the Raman analysis at high spatial resolution, an area of 8 by 8 μm^2 was mapped with a data point every 0.33 μm. To generate an image showing the distribution of ethene-rich material in the matrix of polypropene, a number of steps were pursued. All individual spectra of the spectral map were smoothed to reduce noise and spikes. Subsequently, the spectra were offset such that the minimum intensity coincided with zero. Figure 15 shows the Raman spectra of polypropene, polyethene, and a random ethene–propene copolymer. The spectral regions used for the construction of the conventional images are highlighted. Ratioing the area under the spectrum around 1296 cm^{-1} over that at 1330 cm^{-1}, as highlighted in Figure 15, yields a composition image in which a high ratio is characteristic for a location in

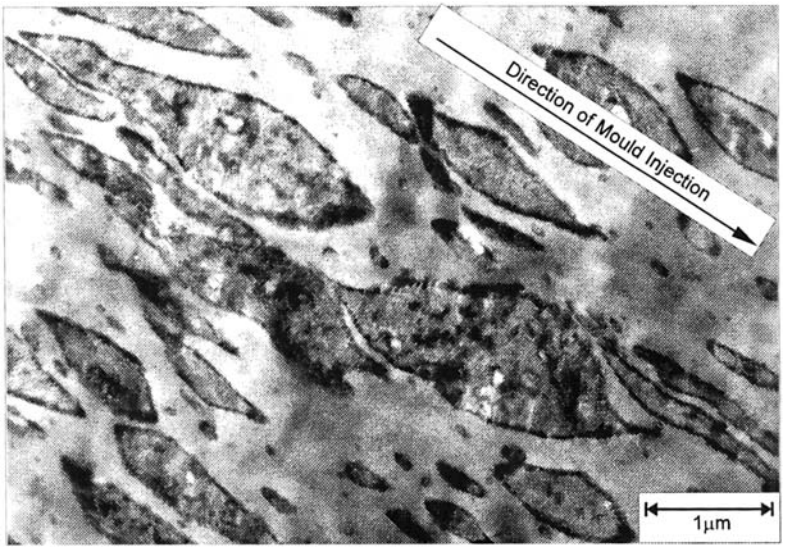

Figure 17 Enlargement of the TEM micrograph of sample *A*. The predominant crystalline species can be recognized by their lamellar structure. The black, featureless regions correspond to the highly stained amorphous region in the sample.

the sample with a high content in ethene-rich components (polyethene and the ethene–propene copolymer).

Figure 18(A) shows a composition image of the sample. Dark shading represents a high concentration of ethene-rich polymer relative to that of polypropene. A corresponding pseudo-3D plot of the relative amounts of ethene-rich to polypropene material is represented in Figure 18(B). Segregated particles of high ethene content can clearly be distinguished in a matrix consisting of predominantly polypropene. Furthermore, the segregated particles appear elongated along the direction of mold injection. From the composition image, the position, shape, and size of the dispersed phase in the imaged area can be determined. It is impossible, though, to deduce the actual composition at the different sampling points of the image. However, the spectra corresponding to the sampling points of the image can be extracted. Figures 18(C) and 18(E) show the spectra extracted at locations of high and low content in ethene-rich polymer, respectively. Spectrum 18(C) is that of almost, though not fully, pure polyethene. A small amount of polypropene is still distinguishable. The spectrum 18(E) is that of pure polypropene. In either case, it is impossible to estimate the amount of copolymer contributing to the spectra. However, the extracted spectra are of very high quality such that curve fitting can be attempted. Weighted curve fitting is used to extract the blend composition at high spatial resolution from the spectra extracted at different positions in the Raman image. The spectra as extracted along the line marked in Figure 18(A) have been fitted, and the corresponding blend composition is plotted in the form of a composition profile in Figure 19(A). The

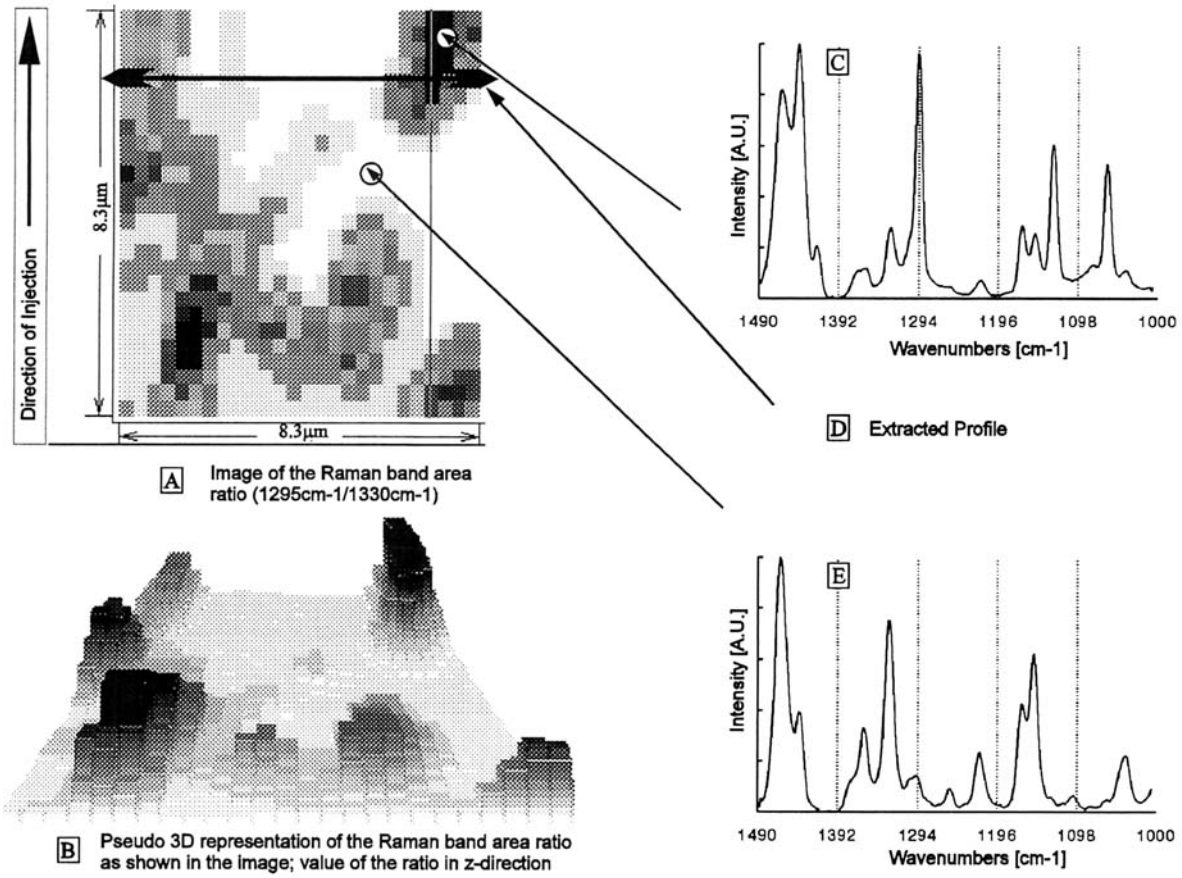

Figure 18 (A) Image of the distribution of ethene-rich polymer in the area covered by the Raman image of blend sample *A* [14.5% polyethene/7.5% (70/30) ethene–propene copolymer/78% polypropene]. A dark color corresponds to high content of ethene-rich polymer with respect to polypropene. (B) Pseudo-3D representation of the image in A. (C) Spectrum extracted at a location of a high content of ethene-rich material. (D) Line along which the spectra were extracted for the preparation of a compositional profile. (E) Spectrum extracted at a location of a low content in ethene-rich material.

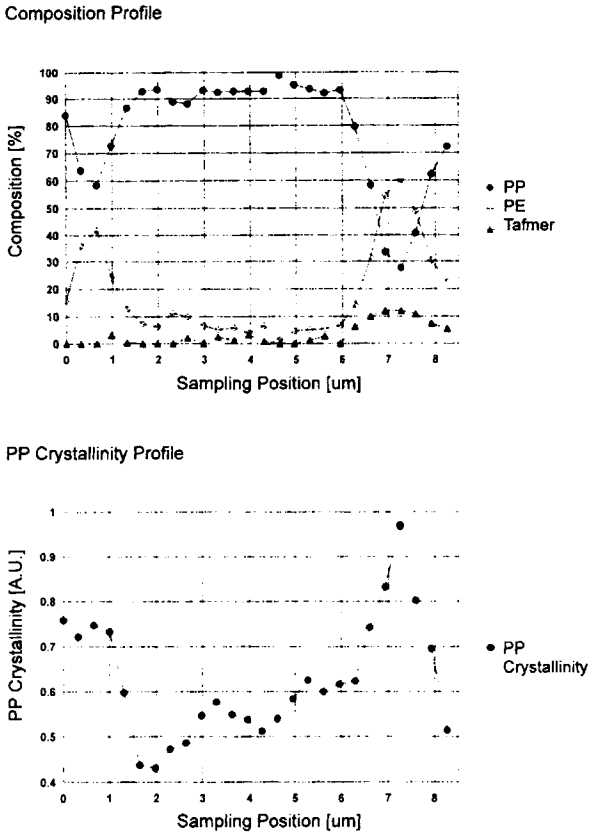

Figure 19 (A) Composition profile as obtained by extracting the spectra from the Raman image of sample *A* along the line depicted in Figure 19(D) and subsequent weighted curve fitting. (B) Polypropene crystallinity profile along the same line. (C) Profile of the ratio of the copolymer content divided by the polyethene content.

composition profile intercepts two locations of a high content of ethene-rich material at the left and at the right-hand edge of the image in Figure 18(A). These correspond to the segregated particles as were witnessed by transmission electron microscopy. The polypropene concentration is drastically reduced at the locations of the segregated phase. Amidst the ethene-rich particles, the polypropene concentration rises to values between 90 and 100%. The ethene-rich segregated particle on the left-hand side consists mainly of polyethene, while that at the right-hand side also contains a significant amount of copolymer. In fact, the copolymer concentration across most of the line extracted from the image is so low that it is well within the error margin. The actual presence of copolymer at such low experimentally determined concentrations cannot be regarded as certain. Only in the segregated particle at the right-hand side is the copolymer concentration above 5% and thus significant. Furthermore, the copolymer concentration rises, peaks, and decreases simultaneously with the polyethene concentration. For a concentration profile intersecting a core/shell structure, a peaking of the copolymer concentration before and after reaching the maximum polyethene concentration would be expected. However, it would be premature to conclude that absence of clear indications for a core/shell structure indicates that the copolymer diffuses on a large scale into the polyethene. The observed concentration profiles for the polyethene and copolymer are more likely due to insufficient spatial resolution of the Raman microscope.

Figure 20 gives a schematic representation of the sampling condition in the thin blend film. A perfectly round core/shell structure is assumed for the dispersed phase. The polyethene is represented as a white particle which is surrounded by the copolymer phase (striped). The segregated phase is positioned in the middle of the sample film. Assuming a film thickness of 2 μm and a diameter of the polyethene particle of 1 μm, the copolymer shell in a pure core/shell structure has to be comparatively thin to still

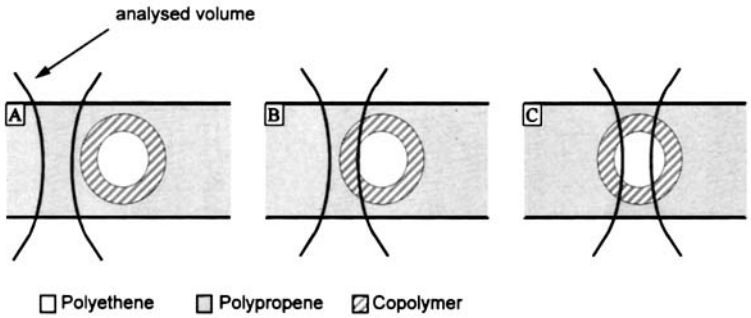

Figure 20 Schematic representation of three characteristic sampling situations that principally might arise during the analysis of a sample film with spherical inclusions of segregated phase by confocal Raman microscopy. The segregated phase consists of two components which are assumed to form a core/shell structure. The analyzed volume is represented by the hourglass-shaped beam profile of the focused laser beam.

maintain the relative polyethene to copolymer ratio used in the blends. For a 2 : 1 polyethene-to-copolymer ratio, the copolymer shell would have a thickness of only 140 nm, while for a 1 : 2 ratio the shell thickness would be of approximately 440 nm. Hence, in any case the imaginary core/shell structure of the segregated phase is completely surrounded by polypropene. If this structure is now probed with the typical hourglass-shaped volume element of analysis of the confocal Raman microscope, three characteristic situations arise. In case A the analyzed volume is fully immersed in the polypropene phase and the Raman spectrum recorded will be that of pure polypropene. In case B the analyzed volume partially includes the copolymer shell of the segregated particle. The Raman spectrum will be that of predominantly polypropene with a minor amount of copolymer. In case C the analyzed volume is focused in the center of the segregated particle. The corresponding Raman spectrum will be that of mainly polyethene with contributions of polypropene and copolymer. However, the simplistic model does not account for the particle shape of the segregated phase, which clearly is not spherical (see transmission electron micrograph in Fig. 16). It also does not consider the case when the segregated particle is not positioned in the middle of the sample film. Furthermore, it is assumed that all copolymer gathers in a shell around the polyethene phase. The possibility that the copolymer forms its own segregated phase is not accounted for. The concentration profile extracted from the Raman image of the sample gives indications for the occurrence of polyethene particles in the polypropene matrix without the presence of any copolymer. The inverse situation of copolymer particles without the presence of any polyethene is probably similarly feasible. This would reduce the amount of copolymer available to form the shells of the model core/shell structure. The shell thickness would consequently be even thinner than predicted by the simplistic model picture. This can also be seen in the transmission micrographs of the sample. The layer of heavily stained amorphous phase around the segregated particle of predominantly polyethene is extremely thin at around 50–100 nm (see Fig. 17). The confocal Raman microscope is not capable of resolving such small structures,[28] and the picture of the copolymer is blurred out. Copolymer phase is detected in areas of the sample directly adjacent to the copolymer phase where there actually is no copolymer. The polyethene and copolymer concentration profiles extracted from the Raman image are therefore neither clearly assignable to a core/shell structure nor to the case of copolymer diffusion into the polyethene phase. The spatial resolution of the confocal Raman microscope is insufficient to distinguish between both models in samples with heterogeneities on submicron dimensions. In the sample analyzed here, the small particle size of the segregated phase and the insufficient spatial resolution of the confocal Raman microscope most likely also account for the observation that the polypropene concentration never drops below 25%. As can be seen from case C of the simplistic model, for insufficiently large particles the polypropene matrix contributes to the Raman spectrum even when the analyzed volume is positioned directly on a copolymer/polyethene particle. This is in line with results reported earlier on the spatial resolving power of the confocal Raman microscope.[28] The lateral spatial resolution under identical experimental conditions was found to be on the order of 1 μm. The depth resolution depended on the type and structure of the sample and was on the order of 2–4 microns. In both cases the resolution was determined as full width at half maximum (FWHM) of a scan of the Raman signal across a defined sample structure in lateral or depth direction, respectively. However, this definition includes that even if two sampling points are separated by the FWHM value, the corresponding spectra will contain contributions of both sampling positions. In our case the thickness of the sample films effectively defines the depth resolution to 2 μm.

In Figure 19(B) the polypropene crystallinity is plotted along the line of extracted spectra from the Raman image of the sample [Fig. 18(D)]. To calculate the polypropene crystallinity, the Raman band area ratio (1167/1152 cm^{-1}) was used. To determine the Raman band area ratios, the contribution to the blend spectra of polyethene at 1170 cm^{-1} and of the copolymers around 1150 cm^{-1} have to be accounted for. The weighted curve-fitting routine, which was used for the determination of the blend composition from the extracted spectra, provided the possibility to extract the contribution of the polypropene in the blend spectrum by weighted subtraction of the other blend components. Figure 21 shows an example of a blend spectrum (thin line) and the remainder after the weighted subtraction of the contribution of the copolymer and the polyethene (thick line). The removal of the copolymer and polyethene contributions appears to be quite good, though it is not perfect. Small residues are left over in the regions of the subtracted blend spectrum that had previously contained strong polyethene bands (i.e., at 1296, 1131, and 1065 cm^{-1}). The changes in the polypropene band cluster at 1167 and 1152 cm^{-1}

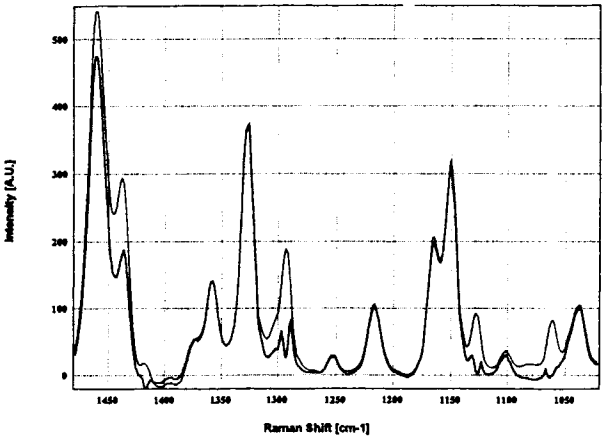

Figure 21 Extraction of the polypropene contribution from the spectrum of a blend of polypropene, polyethene, and ethene–propene copolymer. The contributions of polypropene, polyethene, and copolymer to the blend spectrum are determined by weighted curve fitting. The contributions of polyethene and copolymer are then removed from the blend spectrum (thin line) by weighted subtraction to leave the polypropene contribution to the blend spectrum as remainder (thick line).

due to the correction for the other components of the blend are small. However, the changes are visible and they are expected to be more pronounced for spectra extracted at locations of higher polyethene and/or copolymer content. The profile of the polypropene crystallinity is surprisingly similar to that of the polyethene concentration. At the locations of high polyethene concentration, the polypropene crystallinity is increased.

There have been earlier reports in literature of the influence of polyethene (LLDPE, LDPE) on the crystallization behavior of polypropene in binary polyethene/polypropene blends.[41,50] In phase-segregated blends of polypropene with minor amounts of polyethene, the crystallization behavior of the polypropene matrix appeared strongly influenced by the number and size of the dispersed polyethene droplets. Upon rapid cooling from the melt, supercooling of the polypropene matrix is generally observed. At the crystallization temperature of the polyethene, the dispersed phase crystallized rapidly, providing nuclei for the crystallization of the continuous polypropene phase. The crystallization temperature for the polypropene increased, and an increase in crystallization rate of the supercooled polypropene phase is observed which is thought to be due to heterogeneous crystallization at the boundaries with the polyethene droplets.[51] The temperature curves recorded during the crystallization of the binary blends featured two crystallization peaks, which were interpreted in terms of two insoluble components. However, the crystallization temperature of the polypropene was found to increase slightly with an increasing concentration in the blend of polyethene. In other words, the polypropene crystallized quicker at higher concentrations of polyethene. If polyethene and polypropene were miscible on a molecular scale, one would expect a drop rather than a rise in polypropene crystallization temperature. According to the principle of the colligative effects, the crystallization temperature of a material drops linearly with the concentration of a molecularly dissolved impurity. Hence, the increase in the polypropene crystallization temperature was interpreted to arise from polyethene in the form of small domains in otherwise pure polypropene. The presence of small polyethene crystals acts as nucleation centers for the polypropene. Similarly, in binary blends with polypropene, some types of ethene–propene copolymers are reported to provide the polypropene matrix with nucleation sites such that more crystalline domains resulted.[41,52] In light of these reports, the apparent similarity between the profiles in Figure 19 of the polyethene concentration and the polypropene crystallinity are interpreted as evidence for induced crystallization in the polypropene by adjacent dispersed phase of polyethene.

CONCLUDING REMARKS

In the course of the Raman imaging analysis of the various polymer samples with the confocal laser line scanner, the scope and the limitations of the technique became apparent. Continuously scanning the laser beam over the sample permits the use of considerably higher laser powers without causing damage to the sample. In comparison to the Raman analysis based on a static beam, the collection time for good signal-to-noise spectra can be shortened and the mapping of large sample areas at high spatial resolution more efficient. However, for light-sensitive samples such as the blend of VLDPE/PBT/PC, the applicable laser power is still extremely low even with a scanning laser beam. The required collection times for light-sensitive samples can be very high such that the stability of the sample, the sample position, and the spectrometer become limiting factors. Nevertheless, an image could be obtained with the line-scanning technique, while it is questionable whether an analysis by static beam Raman microscopy with an equally high resolution could be performed without sample burning at all. However, us-

ing the intense, highly focused laser beam of a Raman microscope can have another drawback. Apart from sample burning, the more subtle effects of sample heating can result. In polymers, even moderate heating may cause considerable changes in morphology without inducing noticeable burning. In particular, for composite samples with black fillers, a noticeable heating effect on the sample structure and thus on the Raman band position and shapes has been found.[53–58] The effects due to heating must be carefully considered to avoid an erroneous interpretation of the Raman spectra of thermally altered samples. A further serious limitation of Raman spectroscopy in general is the interference of fluorescence when using visible light for the excitation of the Raman scatter. Under such conditions, a low level of fluorescence is almost omnipresent in polymer samples and can seriously hamper the collection of the very weak Raman light. However, it was shown previously that Raman imaging of weak fluorescent samples was successful in most cases when using the specific advantages of the confocal laser line-scanning technique.[28]

The feasibility to study phase segregation phenomena in polymer blends consisting of chemically very different polymers was demonstrated here. Principally, the study of phase separation in polymer blends of components with almost identical chemical structure (i.e., blends of different types of polyethene) could be attempted based on different degrees of crystallinity in the different phases. If the crystalline lamellar size is different for the different blend components, a separation by the longitudinal acoustic mode (LAM) in the Raman spectrum could be imagined. Alternatively, the Raman imaging of two structurally almost identical polymer components in a blend should conveniently be possible by using isotopically tagged polymers. Additional applications of Raman imaging in polymer science can be envisaged in the study of impurities in a sample (i.e., catalyst rests in polymers) and additives such as pigments and fillers. Moreover, it can be used for the indirect determination of physical parameters which are otherwise difficult to access. The determination of the refractive index profile in an optical fiber via the analysis of the composition profile was shown. Furthermore, the morphological analysis of the individual components of a blend at high spatial resolution was feasible. The contactless mapping of local temperature or pressure differences in otherwise homogeneous samples by the imaging of Raman band positions could equally be envisaged.[30,34,59]

Hence, despite the aforementioned limitations, confocal Raman imaging is a very promising technique for the analysis of polymeric samples with heterogeneities on a size scale of 1 μm or larger. In such samples, the compositional and morphological structure can be studied to a detail which is impossible by alternative techniques. The different constituents of a blend can be identified and quantified at each location of the image, and the compositional and morphological structure of the probed sample area can be made visible as 2D or 3D representation. The structures in these representations compare well with those seen in TEM micrographs at comparable resolution with the bonus of additional chemical information. Hence, this relatively novel technique helps to close the gap between infrared microscopy, with its comparatively poor spatial resolution, on the one hand, and TEM, with its limited chemical information, on the other hand. For heterogeneities on a submicron scale, the resolving power of the Raman microscope is insufficient. For such samples, the value of Raman imaging is limited to the determination of average information.

The DSM management is acknowledged for their permission to publish this work. The authors are grateful to E. Da Silva and B. Roussel, Dilor S. A., for their kind invitation to use their Raman equipment and for many helpful discussions. R. Meier, DSM Research, is gratefully acknowledged for proofreading the manuscript and for helpful comments. K. Reichelt (TU Dresden), W. Bunge, C. Bastiaansen, and P. Elemans (DSM Research) are thanked for provision of samples. Many thanks also to the DSM microscopy department for preparing the samples according to our specifications.

REFERENCES

1. S. Dansei and R. Porter, *Polymer,* **19,** 448 (1978).
2. S. Hobbs, M. Dekkers, and V. Watkins, *Polymer,* **29,** 1598 (1988).
3. M. Baer, *J. Appl. Polym. Sci.,* **16,** 1109 (1972).
4. W. Speri and G. Patrick, *Polymer Eng. Sci.,* **15,** 668 (1975).
5. R. Dickie, *Polymer Blends—Volume 1,* Chap. 8: "Mechanical Properties (Small Deformations) of Multiphase Polymer Blends," D. Paul and S. Newman, Eds., Academic Press, New York, 1978, p. 353.
6. J. Manson and L. Sperling, *Polymer Blends and Composites,* Plenum Press, New York, 1976.
7. P. Painter, M. Coleman, and J. Koenig, *The Theory of Vibrational Spectroscopy and Its Application to Polymeric Systems,* John Wiley, New York, 1982.
8. H. Siesler and K. Holland-Moritz, *Infrared and Raman Spectroscopy of Polymers,* Marcel Dekker, New York, 1980.

9. D. Bower and W. Maddams, *The Vibrational Spectroscopy of Polymers,* Cambridge University Press, Cambridge, 1989.
10. J. Pawley, in *Handbook of Biological Confocal Microscopy,* J. Pawley, Ed., Chap. 2, Plenum Press, New York, 1990, p. 15.
11. G. Rosasco, E. Etz, and W. Cassatt, *Appl. Spectr.,* **29,** 396 (1975).
12. M. Delhaye and P. Dhamelincourt, *J. Raman Spectr.,* **3,** 33 (1975).
13. B. Cook and J. Loudon, *J. Raman Spectr.,* **8,** 249 (1979).
14. P. Dhamelincourt, J. Barbillat, and M. Delhaye, *Spectrosc. Europe,* **5**(2), 16 (1993).
15. P. Hendra, C. Jones, and G. Warnes, *Fourier Transform Raman Spectroscopy: Instrumentation and Applications,* Ellis Horwood, Ellis Horwood Series in Analytical Chemistry, New York, 1991.
16. R. Tabaksblat, R. Meier, and B. Kip, *Appl. Spectr.,* **46,** 60 (1992).
17. G. Cox, *Micron,* **24**(3), 237 (1993).
18. E. Etz and J. Blaha, *National Bureau of Standards Special Publication 533,* U.S. Government Printing Office, Washington DC, 1980, p. 153.
19. D. Gardiner and P. Graves, *Practical Raman Spectroscopy,* Springer-Verlag, Berlin, 1989.
20. G. Puppels, G. DeMul, C. Otto, J. Greve, M. Robert-Nicoud, D. Arndt-Jovin, and T. Jovin, *Nature,* **347,** 301 (1990).
21. *Theory and Practice of Confocal Microscopy,* T. Wilson and C. Sheppard, Eds., Academic Press, New York, 1984.
22. *Confocal Microscopy,* T. Wilson, Ed., Academic Press, London, 1990.
23. R. Meier and B. Kip, *Microbeam Anal.,* **3,** 61. (1994).
24. J. Pastor, *Macromol. Chem.,* Macromol. Symp., **52,** 57 (1991).
25. G. Puppels, M. Grond, and J. Greve, *Appl. Spectrosc.,* **47,** 1256 (1993).
26. P. Treado and M. Morris, *Spectrochim. Acta Rev.,* **13,** 355 (1990).
27. D. Batchelder, B. Smith, S. Webster, and C. Cheng, *Proceedings of the 27th Annual Meeting of MAS,* G. Bailey, Ed., San Francisco Press, 1992.
28. L. Markwort, B. Kip, E. Da Silva, and B. Roussel, *Appl. Spectrosc.,* **49,** 1411 (1995).
29. J. Barbillat, M. Delhaye, and P. Dhamelincourt, *Microbeam Analysis,* G. Bailey, G. Bentley, and J. Small, Eds., San Francisco Press, 1992, p. 1514.
30. W. Carrington, K. Fogarty, L. Lifschitz, and F. Fay, *Handbook of Biological Confocal Microscopy,* J. Pawley, Ed., Chap. 14, Plenum Press, New York, 1990, p. 151.
31. H. Sono, T. Usami, and H. Nakagawa, *Polymer,* **27,** 1497 (1986).
32. H. Kammer, *Acta Polymerica,* **37,** 1 (1986).
33. H. Beyer and H. Riesenberg, *Handbuch der Mikroskopie,* VEB Verlag Technik, Berlin, 1988, p. 188.
34. D. Gardiner, M. Bowden, and B. Graves, *Phil. Trans. R. Soc. Lond.,* **320,** 295 (1986).
35. M. Scheepers, J. Gelan, R. Carleer, P. Adriaensens, D. Vanderzande, B. Kip, and P. Brandts, *Vibr. Spectr.,* **6,** 55 (1993).
36. M. Scheepers, R. Meier, L. Markwort, and B. Kip, *Vibr. Spectr.,* **9,** 139 (1995).
37. L. Boogh, R. Meier, H. Kausch, and B. Kip, *J. Polym. Sci.,* **B30,** 325 (1992).
38. K. Dao, *Polymer,* **25,** 1527 (1984).
39. P. Prentice, E. Papapostolou, and J. Williams, *Polym. Mater. Sci. Eng.,* **51,** 635 (1984).
40. L. Leibler and G. Fredrickson, *Chemistry in Britain,* **1,** 42 (1995).
41. B. Kim, M. Kim, K. Kim, and M. Ha, *Polymer (Korea),* **13,** 157 (1989).
42. M. Coleman and P. Painter, *J. Macromol. Sci. Rev., Macromol. Chem.,* **C16**(2), 197 (1978).
43. J. Chalmers, H. Edwards, J. Lees, D. Long, M. Mackenzie, and H. Willis, *J. Raman Spectrosc.,* **22,** 613 (1991).
44. P. McAllister, T. Carter, and R. Hinde, *J. Polym. Sci.: Polym. Phys.,* **16,** 49 (1978).
45. G. Fraser, P. Hendra, S. Watson, M. Gall, H. Willis, and M. Cudby, *Spectrochimica Acta,* **29A,** 1525 (1973).
46. M. Ize-Iyamu, *Mat. Res. Bull.,* **18,** 225 (1983).
47. K. Tashiro, S. Minami, G. Wu, and M. Kobayashi, *J. Polym. Sci. B: Polym. Phys.,* **30,** 1143 (1992).
48. M. Ize-Iyamu, *Polym. Bull.,* **12,** 487 (1984).
49. B. Armstrong, *J. Quant. Spectrosc. Radiat. Transfer,* **7,** 61 (1967).
50. J. Gunderson and S. Chilcote, *Polym. Mater. Sci. Eng.,* **64,** 393 (1991).
51. Xiao-Qi Zhou and J. Hay, *Polymer,* **34,** 4710 (1993).
52. B. Pukansky, F. Tudos, A. Kallo, and G. Bodor, *Polymer,* **30,** 1399 (1989).
53. I. Robinson, M. Zakikhani, R. Day, and R. Young, *J. Mater. Sci. Lett.,* **6,** 1212 (1987).
54. H. Sakata, G. Dresselhaus, M. Dresselhaus, and M. Endo, *J. Appl. Phys.,* **63,** 2769 (1988).
55. C. Galiotis and D. Batchelder, *J. Mater. Sci. Lett.,* **7,** 545 (1988).
56. J. Ager, K. Veirs, J. Shamir, and G. Rosenblatt, *J. Appl. Phys.,* **68,** 3598 (1990).
57. N. Everall and J. Lumsdon, *J. Mater. Sci.,* **26,** 5269 (1991).
58. N. Everall, J. Lumsdon, and D. Christopher, *Carbon,* **29,** 133 (1991).
59. M. Bowden, G. Dickson, D. Gardiner, and D. Wood, *Appl. Spectrosc.,* **44,** 1679 (1990).

Received August 3, 1995
Accepted December 3, 1995